

Potential Energy Surface for Activation of Methane by Pt⁺: A Combined Guided Ion Beam and DFT Study

Xiao-Guang Zhang, Rohana Liyanage, and P. B. Armentrout*

Contribution from the Department of Chemistry, University of Utah, Salt Lake City, Utah 84112-0850

Received February 12, 2001

Abstract: A guided-ion beam tandem mass spectrometer is used to study the reactions of Pt⁺ with methane, PtCH₂⁺ with H₂ and D₂, and collision-induced dissociation of PtCH₄⁺ and PtCH₂⁺ with Xe. These studies experimentally probe the potential energy surface for the activation of methane by Pt⁺. For the reaction of Pt⁺ with methane, dehydrogenation to form PtCH₂⁺ + H₂ is exothermic, efficient, and the only process observed at low energies. PtH⁺, formed in a simple C–H bond cleavage, dominates the product spectrum at high energies. The observation of a PtH₂⁺ product provides evidence that methane activation proceeds via a (H)₂PtCH₂⁺ intermediate. Modeling of the endothermic reaction cross sections yields the 0 K bond dissociation energies in eV (kJ/mol) of $D_0(\text{Pt}^+-\text{H}) = 2.81 \pm 0.05$ (271 ± 5), $D_0(\text{Pt}^+-2\text{H}) = 6.00 \pm 0.12$ (579 ± 12), $D_0(\text{Pt}^+-\text{C}) = 5.43 \pm 0.05$ (524 ± 5), $D_0(\text{Pt}^+-\text{CH}) = 5.56 \pm 0.10$ (536 ± 10), and $D_0(\text{Pt}^+-\text{CH}_3) = 2.67 \pm 0.08$ (258 ± 8). $D_0(\text{Pt}^+-\text{CH}_2) = 4.80 \pm 0.03$ eV (463 ± 3 kJ/mol) is determined by measuring the forward and reverse reaction rates for $\text{Pt}^+ + \text{CH}_4 \rightleftharpoons \text{PtCH}_2^+ + \text{H}_2$ at thermal energy. We find extensive hydrogen scrambling in the reaction of PtCH₂⁺ with D₂. Collision-induced dissociation (CID) of PtCH₄⁺, identified as the H–Pt⁺–CH₃ intermediate, with Xe reveals a bond energy of 1.77 ± 0.08 eV (171 ± 8 kJ/mol) relative to Pt⁺ + CH₄. The experimental thermochemistry is favorably compared with density functional theory calculations (B3LYP using several basis sets), which also establish the electronic structures of these species and provide insight into the reaction mechanism. Results for the reaction of Pt⁺ with methane are compared with those for the analogous palladium system and the differences in reactivity and mechanism are discussed.

Introduction

There are numerous studies of the reactions of atomic first-row and second-row transition metal ions (M⁺) with hydrogen and small hydrocarbons in the gas phase, i.e., in the absence of solvent, stabilizing ligands, and metal supports.^{1,2} Such studies provide insight into the electronic requirements for the activation of H–H, C–H, and C–C bonds by single metal centers and periodic trends in the reactivity of metals. The guided ion beam methods used in our laboratory have the particular strength that they allow derivation of M⁺–H and M⁺–C_nH_m, $n = 1-3$, $m = 0 - (2n + 2)$, bond dissociation energies (BDEs).² The thermochemistry obtained from these studies is of obvious fundamental interest and also has implications in understanding a variety of catalytic reactions involving transition metal systems.^{3,4} In addition, these relatively small systems form an ideal interface between experiment and theory. Comparable gas-phase studies are less extensive for third-row transition-metal cations, although there are a number of experimental^{5–13} and

theoretical^{8–10,14–21} studies in the literature. To provide more detailed information on such systems, an ongoing project in our laboratory is to use guided ion beam tandem mass spectrometry to systematically study the activation of H–H, C–H, and C–C bonds by the third-row transition metal cations.

In this work, we report results for several reactions that probe the potential energy surface for activation of methane by Pt⁺. It is well-known that platinum is one of the most versatile and

(1) Allison, J. *Prog. Inorg. Chem.* **1986**, *34*, 627. Squires, R. R. *Chem. Rev.* **1987**, *87*, 623. *Gas-Phase Inorganic Chemistry*; Russell, D. H., Ed.; Plenum: New York, 1989. Eller, K.; Schwarz, H. *Chem. Rev.* **1991**, *91*, 1121.

(2) For recent reviews, see: (a) Armentrout, P. B.; Kickel, B. L. In *Organometallic Ion Chemistry*; Freiser, B. S., Ed.; Kluwer: Dordrecht, 1996; p 1. (b) Armentrout, P. B. In *Topics in Organometallic Chemistry*; Brown, J. M., Hofmann, P., Eds.; Springer-Verlag: Berlin, 1999; Vol. 4-1, p 1.

(3) Crabtree, R. H. *The Organometallic Chemistry of the Transition Metals*, 2nd ed.; John Wiley & Sons: New York, 1994.

(4) Somorjai, G. A. *Introduction to Surface Chemistry and Catalysis*; John Wiley & Sons: New York, 1994.

(5) Sunderlin, L. S.; Armentrout, P. B. *J. Am. Chem. Soc.* **1989**, *111*, 3845.

(6) Irikura, K. K.; Beauchamp, J. L. *J. Phys. Chem.* **1991**, *95*, 8344.

(7) Wesendrup, R.; Schröder, D.; Schwarz, H. *Angew. Chem., Int. Ed. Engl.* **1994**, *33*, 1174.

(8) Heinemann, C.; Wesendrup, R.; Schwarz, H. *Chem. Phys. Lett.* **1995**, *239*, 75.

(9) Pavlov, M.; Blomberg, M. R. A.; Siegbahn, P. E. M.; Wesendrup, R.; Heinemann, C.; Schwarz, H. *J. Phys. Chem. A* **1997**, *101*, 1567.

(10) Achatz, U.; Beyer, M.; Joos, S.; Fox, B. S.; Niedner-Schatteburg, G.; Bondybey, V. E. *J. Phys. Chem. A* **1999**, *103*, 8200.

(11) Achatz, U.; Berg, C.; Joos, S.; Fox, B. S.; Beyer, M. K.; Niedner-Schatteburg, G.; Bondybey, V. E. *Chem. Phys. Lett.* **2000**, *320*, 53.

(12) Buckner, S. W.; MacMahon, T. J.; Byrd, G. D.; Freiser, B. S. *Inorg. Chem.* **1989**, *28*, 3511.

(13) Ranasinghe, Y. A.; MacMahon, T. J.; Freiser, B. S. *J. Phys. Chem.* **1991**, *95*, 7721.

(14) Irikura, K. K.; Goddard, W. A., III *J. Am. Chem. Soc.* **1994**, *116*, 8733.

(15) Heinemann, C.; Koch, W.; Schwarz, H. *Chem. Phys. Lett.* **1995**, *245*, 509.

(16) Heinemann, C.; Hertwig, R. H.; Wesendrup, R.; Koch, W.; Schwarz, H. *J. Am. Chem. Soc.* **1995**, *117*, 495.

(17) Holthausen, M. C.; Heinemann, C.; Cornehl, H. H.; Koch, W.; Schwarz, H. *J. Chem. Phys.* **1995**, *102*, 4931.

(18) Heinemann, C.; Schwarz, H.; Koch, W.; Dyal, K. G. *J. Chem. Phys.* **1996**, *104*, 4642.

(19) Ohanessian, G.; Brusich, M. J.; Goddard, W. A., III *J. Am. Chem. Soc.* **1990**, *112*, 7179.

(20) Musaev, D. G.; Morokuma, K. *Isr. J. Chem.* **1993**, *33*, 307.

(21) Perry, J. K.; Ohanessian, G.; Goddard, W. A. *Organometallics* **1994**, *13*, 1870.

all-purpose metal catalysts,^{3,4} whereas methane is the most inert hydrocarbon and a plentiful feedstock in the chemical industry. Several experimental^{6–10} and theoretical^{8–10,14–19} studies on the activation of methane by Pt⁺ have been reported in the literature. Irikura and Beauchamp demonstrated that several “naked” third-row transition metal cations are capable of dehydrogenating methane at thermal energies to yield the methyldiene complexes, MCH₂⁺.⁶ Schwarz, Siegbahn, and co-workers have performed combined theoretical and experimental studies on the Pt⁺-mediated activation of methane.^{8,9} They showed that the dehydrogenation of CH₄ by thermalized Pt⁺ cations proceeds along a doublet ground-state potential energy surface and is reversible (Pt⁺ + CH₄ ⇌ PtCH₂⁺ + H₂) under the thermal conditions in a Fourier transform ion-cyclotron resonance (FTICR) mass spectrometry. Bondybey and co-workers¹⁰ found that the thermal reactions of methane with Pt⁺ or PtAr⁺ lead to the formation of PtCH₂⁺. In contrast, ligand-exchange reactions, in which up to four argon ligands are replaced by methane, are observed for PtAr_m⁺, *m* = 2–6, at thermal energies. No isotopic scrambling was observed for the reactions of PtCH₄⁺ with CD₄ and PtCD₄⁺ with CH₄. In addition, theoretical calculations have predicted the BDEs of Pt⁺–H,¹⁹ Pt⁺–CH₂,^{9,10,14–16,18} and Pt⁺–CH₃;¹⁷ however, only the Pt⁺–CH₂ bond energy has been measured experimentally in the literature.^{8,9}

One of the challenging problems in the study of alkane activation by transition metal ions is to determine the reaction mechanism. All previous experimental studies concerning the reaction of Pt⁺ with methane were performed at thermal energies,^{6–10} such that dehydrogenation was the only process observed. On the basis of ab initio calculations,^{8–10} the reaction mechanism is postulated to involve Pt⁺ insertion into one C–H bond of CH₄ as the initial step followed by α-H transfer and then the reductive elimination of H₂. However, the previous experiments cannot supply complete and quantitative information about the potential energy surface of the PtCH₄⁺ system except for energetics of the PtCH₂⁺ + H₂ channel.^{8,9} In the present study, we investigate the reactions of Pt⁺ with CH₄ and CD₄, PtCH₂⁺ with H₂ and D₂, and collision-induced dissociation (CID) of PtCH₄⁺ and PtCH₂⁺ with Xe over a wide range of kinetic energies. We examine both exothermic and endothermic processes, thereby allowing the determination of several bond energies, probing the potential energy surface, and providing mechanistic information complementary to previous works.^{6–10} Finally, we compare the reactivity and mechanism of the platinum system with those of its congener in the second transition metal series, the palladium system.²²

Experimental Section

General Procedures. The guided ion beam mass spectrometer on which these experiments were performed has been described in detail previously.^{23,24} Briefly, Pt⁺ ions are generated in a direct current discharge flow tube source described below, extracted from the source, accelerated, and focused into a magnetic sector momentum analyzer for mass analysis. The mass-selected ions are decelerated to a desired kinetic energy and focused into an octopole ion beam guide that uses radio frequency electric fields to trap the ions in the radial direction and ensure complete collection of reactant and product ions.^{25,26} The octopole passes through a static gas cell with an effective length of

8.26 cm that contains the neutral collision/reaction partner at a low pressure (usually less than ~0.3 mTorr) so that multiple ion–molecule collisions are improbable. All products reported here result from single bimolecular encounters, as verified by pressure dependence studies. The unreacted parent and product ions are confined radially in the guide until they drift to the end of the octopole where they are extracted, focused, and passed through a quadrupole mass filter for mass analysis. Ions are subsequently detected with a secondary electron scintillation ion detector using standard pulse counting techniques. Reaction cross sections are calculated from product ion intensities relative to reactant ion intensities after correcting for background signals.²⁷ Uncertainties in absolute cross sections are estimated to be ±20%.

The kinetic energy of the ions is varied in the laboratory frame during the experiment by scanning the dc bias on the octopole rods with respect to the potential of the ion source region. Laboratory (lab) ion energies are converted to energies in the center-of-mass frame (CM) by using the formula $E_{CM} = E_{lab}m/(m + M)$, where *m* and *M* are the neutral and ionic reactant masses, respectively. Two effects broaden the cross section data: the kinetic energy distribution of the reactant ion and the thermal motion of the neutral reactant gas (Doppler broadening).²⁸ The absolute zero and the full width at half-maximum (fwhm) of the kinetic energy distribution of the reactant ions are determined using the octopole beam guide as a retarding potential analyzer, as described previously.²⁷ The distributions of ion energies, which are independent of energy, are nearly Gaussian and have a typical fwhm of 0.3–0.6 eV (lab) in these studies. Uncertainties in the absolute energy scale are ±0.05 eV (lab).

Ion Source. Pt⁺ ions are produced in a direct current discharge flow tube (DC/FT) source,²⁴ consisting of a cathode held at high negative voltage (0.7–1.5 kV) over which a flow of approximately 90% He and 10% Ar passes at a total pressure of 0.3–0.4 Torr and ambient temperature. In this work, the cathode is platinum foil attached to an iron holder. Ar⁺ ions created in the discharge are accelerated toward the platinum cathode, thereby sputtering Pt⁺. Pt⁺ ions are then swept down a one-meter long flow tube and undergo ~10⁵ thermalizing collisions with He and ~10⁴ collisions with Ar before entering the guided ion beam apparatus. Trace amounts of low-lying excited states of Pt⁺ are observed to survive these flow conditions, as found by examining the test reaction of Pt⁺ with O₂.²⁹ These excited species are easily removed by introducing O₂ to the flow tube about 15 cm downstream of the discharge zone at a pressure of ~150 mTorr. With the addition of such a cooling gas, the DC/FT source produces metal ions in the ground state. For example, on the basis of comparisons to a surface ionization source, the DC/FT source was found to generate Sc⁺,³⁰ Fe⁺,³¹ Co⁺,³² Ni⁺,³³ Ru⁺,³⁴ Rh⁺,³⁴ and Pd⁺ ions with an average electronic temperature of 700 ± 400 K, and Y⁺, Zr⁺, Nb⁺, and Mo⁺ ions with an average electronic temperature of 300 ± 100 K.³⁵ Therefore, Pt⁺ ions created under such conditions are believed to be in the ground ²D_{5/2}(5d⁹) electronic state term. Even at 1100 K, the population of the lowest-lying excited electronic term, ⁴F_{9/2} at 0.593 eV,³⁶ is only 0.3%, such that 99.7% of the ions are in the ²D_{5/2} ground state. Thus, the average electronic energy at this temperature is only 0.002 eV. This is consistent with the failure to observe any evidence for electronically excited Pt⁺ species in the present or related studies^{29,37} once the O₂ cooling gas is added to the flow tube.

PtCH₂⁺ and PtCH₄⁺ are produced by the introduction of CH₄ into the flow tube about 15 cm downstream of the discharge zone at a

(27) Ervin, K. M.; Armentrout, P. B. *J. Chem. Phys.* **1985**, *83*, 166.

(28) Chanry, P. J. *J. Chem. Phys.* **1971**, *55*, 2746.

(29) Zhang, X.-G.; Armentrout, P. B. Work in progress.

(30) Kickel, B. L.; Armentrout, P. B. *J. Am. Chem. Soc.* **1995**, *117*, 4057.

(31) Clemmer, D. E.; Chen, Y.-M.; Khan, F. A.; Armentrout, P. B. *J. Phys. Chem.* **1994**, *98*, 6522.

(32) Haynes, C. L.; Armentrout, P. B. *Organometallics* **1994**, *13*, 3480.

(33) Kickel, B. L.; Armentrout, P. B. *J. Am. Chem. Soc.* **1995**, *117*, 764.

(34) Chen, Y.-M.; Elkind, J. L.; Armentrout, P. B. *J. Phys. Chem.* **1995**, *99*, 10438.

(35) Sievers, M. R.; Chen, Y.-M.; Armentrout, P. B. *J. Phys. Chem.* **1996**, *100*, 54.

(36) Moore, C. E. *Atomic Energy Levels*; NSRDS-NBS: Washington, DC, 1971, 35/Vol. III.

(37) Zhang, X.-G.; Shin, S.-Y.; Rue, C.; Armentrout, P. B. Work in progress.

(22) Chen, Y.-M.; Sievers, M. R.; Armentrout, P. B. *Int. J. Mass Spectrom. Ion Processes* **1997**, *167/168*, 195.

(23) Loh, S. K.; Hales, D. A.; Lian, L.; Armentrout, P. B. *J. Chem. Phys.* **1989**, *90*, 5466.

(24) Schultz, R. H.; Armentrout, P. B. *Int. J. Mass Spectrom. Ion Processes* **1991**, *107*, 29.

(25) Teloy, E.; Gerlich, D. *Chem. Phys.* **1974**, *4*, 417.

(26) Gerlich, D. *Adv. Chem. Phys.* **1992**, *82*, 1.

pressure of ~ 2 mTorr. Three-body collisions with the He/Ar flow gas stabilize and thermalize the ions both rotationally and vibrationally. We assume that these ions are in their ground electronic states and that the internal energy of these clusters is well described by a Maxwell–Boltzmann distribution of rotational and vibrational states corresponding to 300 ± 100 K. Previous studies from this laboratory have shown that these assumptions are usually valid for molecular species.²

Data Analysis. The kinetic-energy dependence of product cross sections is analyzed to determine E_0 , the energy threshold for product formation at 0 K. E_0 differs from the apparent threshold observed under laboratory conditions because of the Maxwell–Boltzmann velocity distribution and internal energy of the neutral reactants, and the kinetic and internal energy distributions of the reactant ions. Each of these contributions allows reactions to occur at energies below E_0 . To determine E_0 , endothermic reaction cross sections are modeled using eq 1,^{2,38,39,40}

$$\sigma(E) = \sigma_0 \sum g_i (E + E_i - E_0)^n / E \quad (1)$$

where σ_0 is an energy-independent scaling factor, E is the relative kinetic energy of the reactants, and n is an adjustable parameter. There is an explicit sum of the contributions from rovibrational states of the reactants at 300 K, denoted by i , having energies E_i and populations g_i , where $\sum g_i = 1$. The various sets of vibrational frequencies and rotational constants used to determine E_i in this work are taken from the literature for H₂,⁴¹ D₂,⁴¹ CH₄,⁴² and CD₄,⁴² and from ab initio calculations for PtCH₂⁺ and HPtCH₃⁺.⁴³ As noted above, the electronic energy of the Pt⁺ reactant is believed to be negligible. Before comparison with the experimental data, eq 1 is convoluted with the kinetic energy distributions of the ions and neutral reactants at 300 K. The σ_0 , n , and E_0 parameters are then optimized using a nonlinear least-squares analysis to give the best reproduction of the data.²⁷ Error limits for E_0 are calculated from the range of threshold values for different data sets over a range of acceptable n values combined with the absolute error in the energy scale.

Theoretical Calculation Section

All quantum chemistry calculations here are computed with the B3LYP hybrid density functional method^{44,45} and performed with the GAUSSIAN 98 suite of programs.⁴⁶ In all cases, the thermochemistry calculated here is corrected for zero-point energy effects. Because several of the transition states of interest here involve bridging hydrogens, the rather large 6-311++G(3df,3p) basis set is used for

(38) Chesnavich, W. J.; Bowers, M. T. *J. Phys. Chem.* **1979**, *83*, 900.

(39) Aristov N.; Armentrout, P. B. *J. Am. Chem. Soc.* **1986**, *108*, 1806.

(40) Armentrout, P. B. In *Advances in Gas-Phase Ion Chemistry*; Adams, N. G.; Babcock, L. M., Eds.; JAI: Greenwich, 1992, Vol. 1, p 83.

(41) Huber, K. P.; Herzberg, G. *Molecular Spectra and Molecular Structure*; Vol. IV, Constants of Diatomic Molecules; Van Nostrand Reinhold: New York, 1979.

(42) Shimanouchi, T. *Tables of Molecular Vibrational Frequencies*; NSRDS-NBS39: Washington, DC, 1972; Consolidated Vol. I, p 1.

(43) Diefenbach, M.; Schwarz, H. Personal communication. For PtCH₂⁺, the vibrational frequencies are 779.5, 780.4, 1054.5, 1436.1, 3077.0, and 3198.3 cm⁻¹; the rotational constants are 9.43, 0.35, and 0.34 cm⁻¹. For PtCH₃⁺, the vibrational frequencies are 76.0, 479.5, 567.0, 794.0, 866.6, 1307.6, 1433.0, 1449.6, 2280.5, 3050.3, 3170.7, and 3193.4 cm⁻¹; the rotational constants are 2.94, 0.26, and 0.25 cm⁻¹.

(44) Becke, A. D. *J. Chem. Phys.* **1993**, *98*, 5648.

(45) Lee, C.; Yang, W.; Parr, R. G. *Phys. Rev. B* **1988**, *37*, 785.

(46) Frisch, M. J.; Trucks, G. W.; Schlegel, H. B.; Scuseria, G. E.; Robb, M. A.; Cheeseman, J. R.; Zakrzewski, V. G.; Montgomery, J. A., Jr.; Stratmann, R. E.; Burant, J. C.; Dapprich, S.; Millam, J. M.; Daniels, A. D.; Kudin, K. N.; Strain, M. C.; Farkas, O.; Tomasi, J.; Barone, V.; Cossi, M.; Cammi, R.; Mennucci, B.; Pomelli, C.; Adamo, C.; Clifford, S.; Ochterski, J.; Petersson, G. A.; Ayala, P. Y.; Cui, Q.; Morokuma, K.; Malick, D. K.; Rabuck, A. D.; Raghavachari, K.; Foresman, J. B.; Cioslowski, J.; Ortiz, J. V.; Baboul, A. G.; Stefanov, B. B.; Liu, G.; Liashenko, A.; Piskorz, P.; Komaromi, I.; Gomperts, R.; Martin, R. L.; Fox, D. J.; Keith, T.; Al-Laham, M. A.; Peng, C. Y.; Nanayakkara, A.; Gonzalez, C.; Challacombe, M.; Gill, P. M. W.; Johnson, B.; Chen, W.; Wong, M. W.; Andres, J. L.; Gonzalez, C.; Head-Gordon, M.; Replogle, E. S.; Pople, J. A. *Gaussian 98*, Revision A.7; Gaussian, Inc., Pittsburgh, PA, 1998.

Table 1. Thermochemical Data at 0 K

species	$\Delta_f H_0^\circ$ (kJ/mol)	species	$\Delta_f H_0^\circ$ (kJ/mol)
H	216.035 \pm 0.006 ^a	D	219.807 \pm 0.004 ^a
C	711.19 \pm 0.46 ^a	CD	592.2 \pm 1.7 ^{s,h}
CH	592.9 \pm 1.7 ^b	CD ₂	385.0 \pm 2.5 ^{s,i}
CH ₂	388.3 \pm 2.5 ^c	CD ₃	141.4 \pm 0.4 ^{s,j}
CH ₃	149.8 \pm 0.4 ^d	CD ₄	-80.3 \pm 0.4 ^{s,k}
CH ₄	-66.4 \pm 0.4 ^{e,f}		

^a Chase, M. W., Jr. *J. Phys. Chem. Ref. Data*, **1998**, Monograph 9, NIST-JANAF Thermochemical Tables, 4th ed. ^b Ervin, K. M.; Gronert, S.; Barlow, S. E.; Gilles, M. K.; Harrison, A. G.; Bierbaum, V. M.; DePuy, C. H.; Lineberger, W. C.; Ellison, G. B. *J. Am. Chem. Soc.* **1990**, *112*, 5750. ^c Leopold, D. G.; Murray, K. K.; Stevens Miller, A. E.; Lineberger, W. C. *J. Chem. Phys.* **1985**, *83*, 4849. ^d Berkowitz, J.; Ellison, G. B.; Gutman, D. *J. Phys. Chem.* **1994**, *98*, 2744. ^e $\Delta_f H_{298}$ value from: Pedley, J. B.; Naylor, R. D.; Kirby, S. P. *Thermochemical Data of Organic Compounds*, 2nd ed.; Chapman and Hall, New York, 1986. ^f Adjusted to 0 K using information in footnote a. ^g Estimated, assuming ideal gas behavior (cf.: Pamidimukkala, K. M.; Rogers, D.; Skinner, G. B. *J. Phys. Chem. Ref. Data*, **1982**, *11* (No. 1), 83.). ^h Vibrational frequencies for CH, CD, H₂, and D₂ are taken from: *Molecular Spectra and Molecular Structure*; Vol. IV, Constants of Diatomic Molecules; Huber K. P., Herzberg, G., Eds.; Van Nostrand Reinhold: New York, 1979. ⁱ Vibrational frequencies for CH₂ and CD₂ are taken from references in footnotes a and l. Two frequencies of CD₂ are estimated from those of CH₂ on the basis of $\omega_{CD_2} = 0.7338\omega_{CH_2}$, $\omega_{CH_2}/\omega_{CD_2} = (\mu_{CD_2}/\mu_{CH_2})^{1/2}$. ^j Vibrational frequencies for CH₃ and CD₃ are taken from the reference in footnote l. ^k Vibrational frequencies for CH₄ and CD₄ are taken from: Shimanouchi, T., Ed. *Tables of Molecular Vibrational Frequencies*; NSRDS-NBS39: Washington, DC, 1972; Consolidated Vol. I, p 1. ^l Jacox, M. E., Ed. *J. Phys. Chem. Ref. Data*; Monograph No. 3 (Vibrational and Electronic Energy Levels of Polyatomic Transient Molecules), NSRDS: Washington, DC, 1994.

carbon and hydrogen. This basis set gives good results for the thermochemistry of methane and dihydrogen, with deviations from experiment (Table 1) of less than 0.08 eV for the bond energies of H–CH₃ (4.406 vs 4.480 eV), H₂–CH₂ (4.666 vs 4.713 eV), H–CH (4.332 vs 4.360 eV), C–H (3.532 vs 3.465 eV), and H–H (4.505 vs 4.478 eV). The 60 core electrons of platinum are described by the relativistic effective core potentials (ECP) of Hay–Wadt (HW),⁴⁷ equivalent to the Los Alamos ECP (LANL2DZ) basis set, and Stuttgart/Dresden (SD).⁴⁸ The HW-ECP is optimized for neutral atoms, whereas the positive charge differentially contracts the s orbitals compared to the d orbitals. Hence, we also used an altered HW-ECP basis set for Pt as described by Ohanessian et al. (HW+).¹⁹ We also performed single-point energy calculations using the HW+-ECP geometries in which the HW-ECP basis set was expanded as described by Pavlov et al. (by uncontracting one s, one p, and one d function and adding one diffuse d function and two f functions)⁹ and we contracted the s orbitals as described by Ohanessian et al. (HW+X). To evaluate the consequences of and need for these various changes in the basis set for Pt⁺, we systematically compare calculations for the HW, HW+, HW+X, and SD ECPs using the same level of theory (B3LYP) and basis set for C and H, 6-311++G(3df,3p).

The splitting between the ²D(5d⁹) ground state and ⁴F(6s¹5d⁸) first excited state is calculated to be 1.102 (HW), 0.682 (HW+), 0.635 (HW+X), and 0.798 eV (SD). These values should be compared with the experimentally determined 0.759 eV excitation between the averages of properly weighted spin–orbit components of the ²D (0.418 eV above the ²D_{5/2} ground state) and ⁴F (1.177 eV above the ²D_{5/2} ground state) terms.³⁶ Note that the contraction of the s orbitals in the HW+-ECP basis set does lead to much better agreement with experiment for this excitation energy. Because our calculations do not explicitly include spin–orbit interactions, all calculations involving an asymptote including Pt⁺ are referenced to the average energy of the spin–orbit components of the ²D term at 0.418 eV. To properly compare to experimental values, which refer to the energy of the ²D_{5/2} ground state at 0.0 eV, the calculated values must be corrected for this different

(47) Hay, P. J.; Wadt, W. R. *J. Chem. Phys.* **1985**, *82*, 299.

(48) Andrae, D.; Hauessermann, U.; Dolg, M.; Stoll, H.; Preuss, H. *Theor. Chim. Acta* **1990**, *77*, 123.

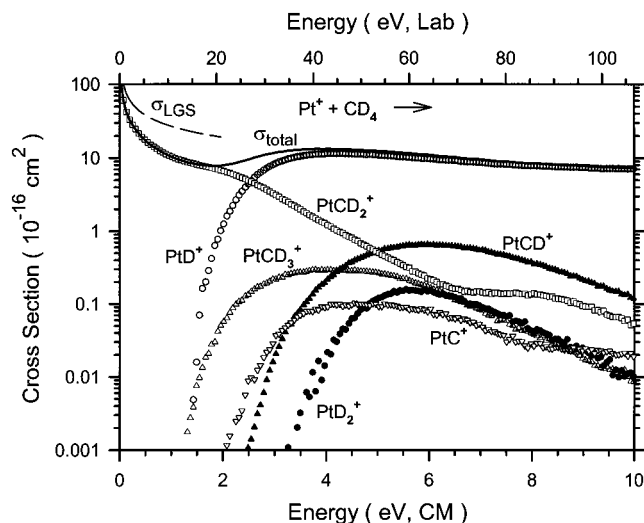
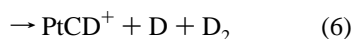
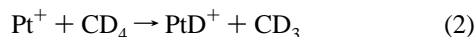


Figure 1. Cross sections for reaction of Pt^+ ($^2D_{5/2}$) with CD_4 as a function of kinetic energy in the center-of-mass frame (lower axis) and laboratory frame (upper axis). The full line shows the total cross section and the dashed line shows the LGS collision cross section.

asymptotic energy. Pavlov et al. make a similar correction (although they reference their energies to the 4F state, which is treated more accurately by the HW-ECP),⁹ but no such correction is mentioned explicitly by Achatz et al.¹⁰ This may explain why their bond energies are systematically higher than comparable ones calculated here and elsewhere.⁹

Experimental Results

Reaction of Pt^+ with Methane. Figure 1 shows cross sections for the bimolecular reaction of $\text{Pt}^+ + \text{CD}_4$, which yields six product ions as shown in reactions 2–7.



Studies of the reaction of Pt^+ with CH_4 were also performed and yielded consistent results for all chemically analogous species. Only results from the perdeuterated methane are presented here because its use reduces mass overlap between product ions, thereby allowing intensities of the various product ions to be measured more accurately over a larger dynamic range.

As can be seen from Figure 1, reactions other than dehydrogenation exhibit thresholds and therefore appear to be endothermic, consistent with previous studies where PtCH_2^+ (PtCD_2^+) is the only ionic product observed in the reaction of Pt^+ with CH_4 (CD_4) under single collision conditions at thermal energies.^{6–10} The cross section for dehydrogenation of CD_4 , to produce PtCD_2^+ , decreases with increasing energy, indicating an exothermic reaction having no barrier in excess of the energy of the reactants. Compared to the Langevin–Gioumousis–Stevenson (LGS) collision cross section,⁴⁹ which has an $E^{-0.5}$

energy dependence, we find that this reaction cross section declines approximately as $E^{-0.7 \pm 0.1}$ below 1.0 eV. For comparison to the literature, our cross sections can be converted to a rate constant by using the following expression, $k(\langle E \rangle) = \nu \sigma(E)$, where $\nu = (2E/\mu)^{1/2}$ and $\mu = mM/(m+M)$, the reduced mass of the reactants. The rate constants depend on the mean energy of the reactants, which includes the average thermal motion of the neutral, such that $\langle E \rangle = E + (3/2)\gamma k_B T$, where $\gamma = M/(m+M)$. For reaction with CH_4 , we obtain $k(0.05 \text{ eV}) = (7.6 \pm 1.7) \times 10^{-10} \text{ cm}^3 \text{ s}^{-1}$, whereas we find $k(0.06 \text{ eV}) = (5.1 \pm 1.1) \times 10^{-10} \text{ cm}^3 \text{ s}^{-1}$ for reaction with CD_4 , at energies slightly higher than thermal, $(3/2)\gamma k_B T = 0.04 \text{ eV}$ at 300 K. These values compare favorably with literature rate constants (all in units of $10^{-10} \text{ cm}^3 \text{ s}^{-1}$) obtained by ion cyclotron resonance (ICR) mass spectrometry of 3.9 ± 1.0 ,⁶ 8.2 ⁸ (which can be adjusted to 5.9 ± 2.5 on the basis of a recalibration of the absolute standard used),⁵⁰ and 4.6 ± 0.3 ¹⁰ for CH_4 , and 3.1 ± 0.8 ⁶ and 2.5 ± 0.3 ¹⁰ for CD_4 . Compared to the LGS collision rate, the reaction with CH_4 occurs at an efficiency of 40–84% (our value is 76%), and with CD_4 , the efficiency is 35–58% (where our value is the upper limit). Our results demonstrate that the rate constants do vary with kinetic energy, which may explain some of the differences in the literature values.

At higher energies ($>2 \text{ eV}$), the PtCD_2^+ cross section declines more quickly. There are several possible decomposition pathways for the PtCD_2^+ product at high energies, which include decomposition into $\text{PtC}^+ + \text{D}_2$, $\text{PtCD}^+ + \text{D}$, and $\text{Pt}^+ + \text{CD}_2$. The magnitudes of the PtC^+ and PtCD^+ channels are too small to account for the decline in the PtCD_2^+ cross section. Decomposition of PtCD_2^+ to $\text{Pt}^+ + \text{CD}_2$ can begin at 4.82 eV, Table 1, which is too high to account for the decline. Therefore, the decrease in the PtCD_2^+ cross section must be attributed to competition with formation of PtD^+ in reaction 2. Such competition is most easily explained if these two reaction channels share a common intermediate, as discussed below.

Formations of PtD^+ and PtCD_3^+ arise from similar apparent thresholds near 1.2 eV, indicating that the $\text{Pt}^+ - \text{D}$ and $\text{Pt}^+ - \text{CD}_3$ single bond energies are similar. Despite the similar energetics, formation of PtD^+ dominates the product spectrum at higher energies. This is because of angular momentum effects, discussed below, and because the PtCD_3^+ product dissociates into $\text{PtCD}^+ + \text{D}_2$. Evidence for the coupling between these two products is the observation that the PtCD^+ product begins to decline between 5 and 6 eV. This is well before it can dissociate into $\text{Pt}^+ + \text{CD}$ (beginning at 9.25 eV, Table 1), and therefore can be attributed to the dissociation of its precursor, PtCD_3^+ , which can begin at $D_0(\text{D}-\text{CD}_3) = 4.58 \text{ eV}$ (Table 1). PtCD_3^+ can also dissociate by loss of a D atom, which accounts for the second feature in the PtCD_2^+ cross section, which becomes evident at $\sim 6.5 \text{ eV}$. Formation of the PtC^+ product must occur by dehydrogenation of the PtCD_2^+ product, as the thermodynamics of this reaction indicate that it is formed in reaction 7 with two D_2 molecules. Further, the PtC^+ cross section starts to decrease at about 5 eV, well before its can dissociate into $\text{Pt}^+ + \text{C}$ (beginning at 8.20 eV, Table 1), because its precursor, PtCD_2^+ , can dissociate into $\text{Pt}^+ + \text{CD}_2$ beginning at 4.80 eV.

The product with the highest threshold is PtD_2^+ , consistent with the formation of the high-energy neutral, CD_2 . A MD_2^+ product is unusual and has not been observed previously in the reactions of methane with first-row and second-row transition metal ions,^{5,22,51–58} or with La^+ or Lu^+ .⁵ PtH_2^+ has been

(50) Schröder, D.; Schwarz, H.; Clemmer, D. E.; Chen, Y.-M.; Armentrout, P. B.; Baranov, V. I.; Bohme, D. K. *Int. J. Mass Spectrom. Ion Processes* **1997**, *161*, 175.

(49) Gioumousis, G.; Stevenson, D. P. *J. Chem. Phys.* **1958**, *29*, 294.

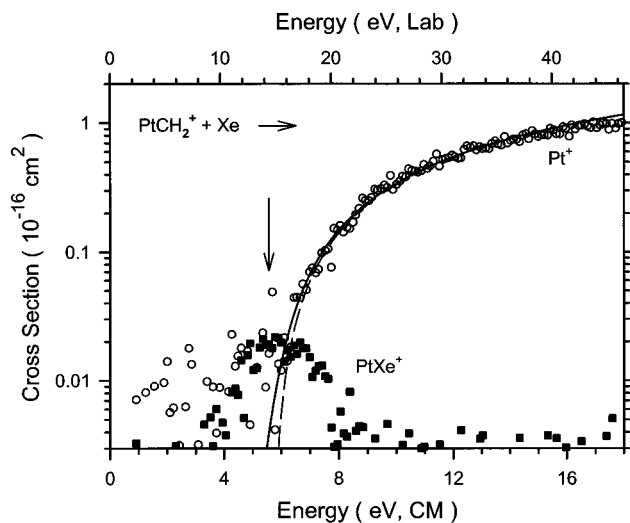
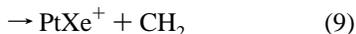


Figure 2. Cross sections for collision-induced dissociation of PtCH₂⁺ with Xe as a function of kinetic energy in the center-of-mass frame (lower axis) and laboratory frame (upper axis). The best fit to the data using eq 1 incorporating RRKM modeling for the reactants with an internal temperature of 0 K is shown as a dashed line. The solid line shows this model convoluted over the kinetic and internal energy distributions of the reactant neutral and ion. The arrow indicates the average threshold energy from all data sets.

observed previously as a product in the reaction of Pt⁺ with dimethyl peroxide.^{9,59} This study also found evidence that the two forms of PtH₂⁺, the dihydride and dihydrogen complexes, may interconvert readily, but do not definitively provide any absolute or relative thermochemical information regarding these forms of PtH₂⁺.

PtCH₂⁺ + Xe. Because the dehydrogenation reaction analogous to process 5 is exothermic, the energy dependence of this process provides no thermochemical information regarding the BDE of Pt⁺–CH₂ except for a lower limit of 4.71 eV = D₀(H₂–CH₂), Table 1. Therefore, we attempted to measure this BDE using a CID experiment. Cross sections for the interaction of Xe with PtCH₂⁺ formed by the reaction of Pt⁺ with CH₄ in the DC/FT source are shown in Figure 2. Two major products are observed and correspond to reactions 8 and 9.



The dominant process, reaction 8, is a simple CID process with an apparent threshold between 5 and 6 eV. A small amount of the ligand exchange process, reaction 9, is also observed. This cross section peaks at the threshold for reaction 8, indicating that the PtXe⁺ product decomposes to Pt⁺ + Xe at higher energies. PtC⁺ was also detected, but its cross section is very noisy because the peak for the PtC⁺ product overlaps with that for the intense PtCH₂⁺ reactant ion beam.

(51) Aristov, N.; Armentrout, P. B. *J. Phys. Chem.* **1987**, *91*, 6178.

(52) Schultz, R. H.; Elkind, J. L.; Armentrout, P. B. *J. Am. Chem. Soc.* **1988**, *110*, 411.

(53) Sunderlin, L. S.; Armentrout, P. B. *J. Phys. Chem.* **1988**, *92*, 1209.

(54) Georgiadis, R.; Armentrout, P. B. *J. Phys. Chem.* **1988**, *92*, 7067.

(55) Haynes, C. L.; Chen, Y.-M.; Armentrout, P. B. *J. Phys. Chem.* **1995**, *99*, 9110.

(56) Chen, Y.-M.; Armentrout, P. B. *J. Phys. Chem.* **1995**, *99*, 10775.

(57) Haynes, C. L.; Chen, Y.-M.; Armentrout, P. B. *J. Phys. Chem.* **1996**, *100*, 111.

(58) Sievers, M. R.; Chen, Y.-M.; Haynes, C. L.; Armentrout, P. B. *Int. J. Mass Spectrom. Ion Processes* **2000**, *195/196*, 149.

(59) Wesendrup, R.; Schalley, C. A.; Schröder, D.; Schwarz, H. *Chem. Eur. J.* **1995**, *1*, 608.

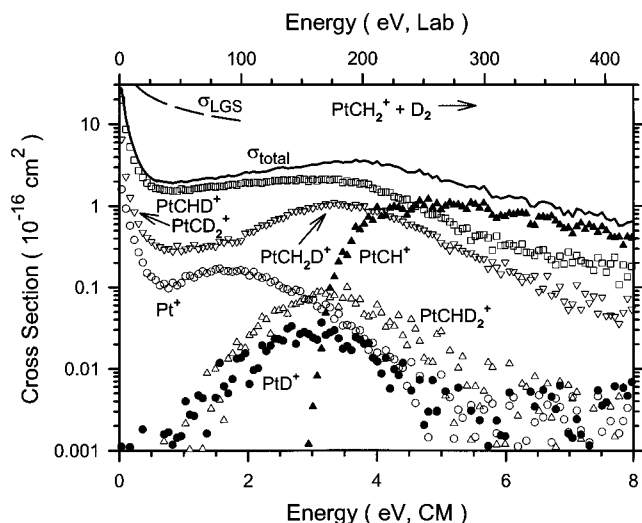
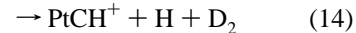
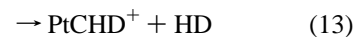
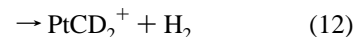


Figure 3. Cross sections for the bimolecular reaction of PtCH₂⁺ with D₂ as a function of kinetic energy in the center-of-mass frame (lower axis) and laboratory frame (upper axis). The full line shows the total cross section and the dashed line shows the LGS collision cross section. As discussed in the text, one product channel can be attributed to the PtCD₂⁺ product at low energies and primarily to PtCH₂D⁺ at higher energies.

PtCH₂⁺ + D₂. Figure 3 shows cross sections for the bimolecular reaction of PtCH₂⁺ with D₂. Seven product ions are observed in reactions 10–16.



We also observe signals for PtC⁺ having a much lower intensity than the PtCH⁺ species but comparable in energy dependence. Similarly, PtH⁺ having an energy dependence like that of PtD⁺ is observed but in lower intensity. These products are not shown in Figure 3 because their absolute magnitudes cannot be established unambiguously as a result of mass overlap from these heavier product ions. Studies of the reaction of PtCH₂⁺ with H₂ were also performed and PtCH₃⁺, PtCH⁺, and Pt⁺ products were found. Only results for PtCH₂⁺ + D₂ are presented here because they permit the hydrogen scrambling reactions 12 and 13 to be observed.

Note that the PtCH₂D⁺ and PtCD₂⁺ product ions have the same mass. However, the PtCD₂⁺ cross section should have a kinetic energy dependence similar to that of PtCHD⁺ and the cross section for PtCH₂D⁺ should be similar to that of PtCHD₂⁺. Further, the absolute magnitude of the PtCH₃⁺ cross section observed in the PtCH₂⁺ + H₂ reaction system is approximately the same magnitude at about 3.5 eV (actually 0.2 Å² larger) compared to that of PtCH₂D⁺ observed in the PtCH₂⁺ + D₂ reaction system. Therefore, the exothermic part of this cross section below 1 eV should be entirely attributable to PtCD₂⁺ and the endothermic part above 1.5 eV should be mainly from PtCH₂D⁺.

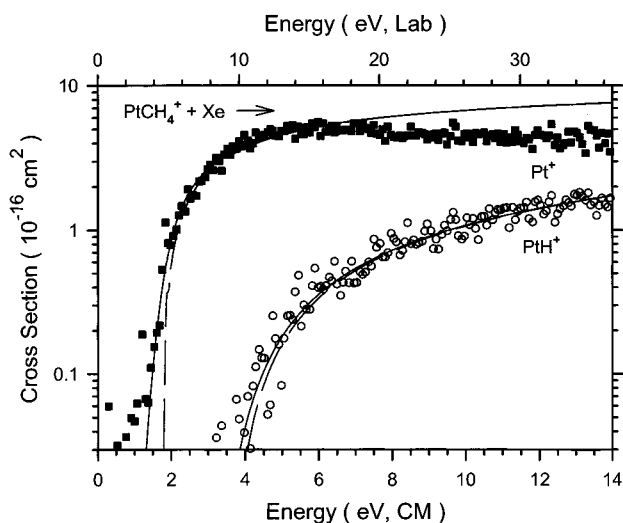


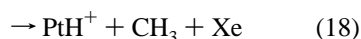
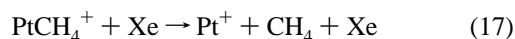
Figure 4. Cross sections for collision-induced dissociation of PtCH_4^+ with Xe (extrapolated to zero pressure) as a function of kinetic energy in the center-of-mass frame (lower axis) and laboratory frame (upper axis). The best fits to the data using eq 1 incorporating RRKM modeling for the reactants with an internal temperature of 0 K are shown as dashed lines. The solid lines show these models convoluted over the kinetic and internal energy distributions of the reactant neutral and ion.

Reactions 12 and 13 are exothermic because of zero-point energy differences. Compared to the Langevin–Gioumousis–Stevenson (LGS) collision cross section,⁴⁹ we find that both reaction cross sections decline approximately as $E^{-1.0}$, respectively, below 0.4 eV. We measure rate constants at thermal energies for reactions 12 and 13 of $(1.4 \pm 0.6) \times 10^{-10}$ and $(3.0 \pm 0.6) \times 10^{-10} \text{ cm}^3 \text{ s}^{-1}$, respectively. These values are close to 0.4×10^{-10} and $1.0 \times 10^{-10} \text{ cm}^3 \text{ s}^{-1}$, respectively, as measured in the ICR experiments of Heinemann et al.⁸

The most interesting observation in this reaction system is that reaction 16 and its perprotio analogue exhibit no obvious energy barriers. As these reactions are the reverse of the dehydrogenation reactions analogous to process 5, this indicates that the reactants and products in the $\text{Pt}^+ + \text{CH}_4 \rightleftharpoons \text{PtCH}_2^+ + \text{H}_2$ reaction system and its deuterated analogues are near equilibrium. We find that the thermal rate constant for reaction 16 is $(0.54 \pm 0.16) \times 10^{-10} \text{ cm}^3 \text{ s}^{-1}$, and the analogous reaction with H_2 has $k = (0.12 \pm 0.03) \times 10^{-10} \text{ cm}^3 \text{ s}^{-1}$. The latter observation agrees with that of Heinemann et al., who found that the reverse reaction has a rate constant of $0.07 \times 10^{-10} \text{ cm}^3 \text{ s}^{-1}$, or 0.5% of the LGS collision rate.⁸

At about 1.5–2 eV, the cross section for the Pt^+ product decreases as the PtCHD_2^+ , PtCH_2D^+ , and PtD^+ cross sections increase, indicating that these channels are coupled to one another. The cross sections of PtCHD_2^+ , PtCH_2D^+ , and PtD^+ start decreasing at about 3.0–3.5 eV, as the PtCH^+ product from reaction 14 increases, suggesting that these channels are also coupled to each other. PtCD^+ might also be a product in such dissociations but it cannot be detected because it has the same nominal mass as the PtCH_2^+ reactant.

$\text{PtCH}_4^+ + \text{Xe}$. Figure 4 shows cross sections for the interaction of Xe with PtCH_4^+ formed by three-body condensation of methane and Pt^+ in the DC/FT source. The two main products are formed in reactions 17 and 18.



The dominant process is loss of methane, reaction 17. Observa-

Table 2. Parameters of Eq 1 Used in Modeling the Reaction Cross Sections

reaction	σ_0	n	E_0 (eV)
$\text{Pt}^+ + \text{CD}_4 \rightarrow \text{PtD}^+ + \text{CD}_3$	14.2 ± 5.1	1.5 ± 0.1	1.90 ± 0.06
$\rightarrow \text{PtD}_2^+ + \text{CD}_2$	0.5 ± 0.3	1.0 ± 0.1	4.08 ± 0.06
$\rightarrow \text{PtCD}_3^+ + \text{D}$	0.5 ± 0.2	1.3 ± 0.1	1.77 ± 0.05
$\rightarrow \text{PtCD}^+ + \text{D}_2 + \text{D}$	2.5 ± 1.7	1.3 ± 0.2	3.58 ± 0.14
$\rightarrow \text{PtC}^+ + 2 \text{D}_2$	0.3 ± 0.1	1.0 ± 0.1	2.80 ± 0.05
$\text{Pt}^+ + \text{CH}_4 \rightarrow \text{PtH}^+ + \text{CH}_3$	14.9 ± 3.4	1.4 ± 0.1	1.76 ± 0.05
$\rightarrow \text{PtH}_2^+ + \text{CH}_2$	1.0 ± 0.4	1.0 ± 0.1	4.05 ± 0.19
$\rightarrow \text{PtCH}_3^+ + \text{H}$	0.4 ± 0.2	1.0 ± 0.1	1.86 ± 0.15
$\rightarrow \text{PtCH}^+ + \text{H}_2 + \text{H}$	1.4 ± 0.1	1.0 ± 0.1	3.57 ± 0.05
$\rightarrow \text{PtC}^+ + 2 \text{H}_2$	0.5 ± 0.1	1.0 ± 0.1	2.64 ± 0.15
$\text{PtCH}_2^+ + \text{D}_2 \rightarrow \text{PtCH}_2\text{D}^+ + \text{D}^a$	1.0 ± 0.8	1.5 ± 0.3	1.73 ± 0.10
$\text{PtCH}_2^+ + \text{H}_2 \rightarrow \text{PtCH}_3^+ + \text{H}$	1.2 ± 0.2	1.4 ± 0.3	1.67 ± 0.11
$\text{PtCH}_4^+ + \text{Xe} \rightarrow \text{Pt}^+ + \text{CH}_4$	4.8 ± 1.0	1.3 ± 0.2	1.72 ± 0.05
$\rightarrow \text{PtH}^+ + \text{CH}_3$	0.3 ± 0.1	1.7 ± 0.2	3.50 ± 0.06
$\text{PtCH}_2^+ + \text{Xe} \rightarrow \text{Pt}^+ + \text{CH}_2$	0.4 ± 0.1	1.7 ± 0.1	5.67 ± 0.16

^a This cross section is modeled after subtracting a power law fit to the low energy part of the cross section attributable to PtCD_2^+ .

tion of reaction 18 is interesting as the CID of MCH_4^+ where $\text{M} = \text{Fe}, \text{Co},$ and Mg yielded only M^+ products.^{60–62} In the present system, two additional minor products, PtXe^+ and PtCH_2^+ , were also observed, but the data are noisy and hence not shown in Figure 4. PtXe^+ has a maximum cross section of $\sim 0.5 \text{ \AA}^2$ near the onset of Pt^+ , and has a cross section that clearly shows endothermic behavior, with an apparent threshold less than 1.0 eV. This behavior is consistent with a $\text{Pt}^+ - \text{Xe}$ bond energy of $0.86 \pm 0.3 \text{ eV}$ recently measured.⁶³ PtCH_2^+ was also detected but the overlap with the intense reactant ion beam, PtCH_4^+ , prevents any sensible information from being extracted from these data. Likewise, it is possible that PtCH_3^+ could have been formed but would not be resolvable from the reactant ions.

Thermochemical and Theoretical Results

The endothermic cross sections in each reaction system are analyzed in detail using eq 1, as described above. The optimum values of the parameters in eq 1 are listed for these systems in Table 2. Because the rotational, vibrational, and translational energy distributions are explicitly included in the modeling, the E_0 thresholds determined using eq 1 correspond to 0 K values. From the thresholds measured, the BDEs for the platinum-ligand cations observed in the reaction of $\text{Pt}^+ + \text{R-L}$ can be calculated using eq 19,

$$D_0(\text{Pt}^+ - \text{L}) = D_0(\text{R-L}) - E_0 \quad (19)$$

where the $D_0(\text{R-L})$ values can be calculated from the heats of formation given in Table 1. This equation assumes that there is no activation barrier in excess of the endothermicity of the reaction, an assumption that is often true for ion–molecule reactions because of the long-range attractive forces.^{2,40} Table 3 provides a summary of the bond energies derived and a comparison with literature values, as discussed below.

$\text{Pt}^+ - \text{H}$. Formation of PtD^+ in reaction 2 has a measured threshold of $1.90 \pm 0.06 \text{ eV}$ (Table 2). This differs appreciably from the apparent threshold for this reaction in Figure 1 because

(60) Schultz, R. H.; Armentrout, P. B. *J. Phys. Chem.* **1993**, *97*, 596.

(61) Haynes, C. L.; Armentrout, P. B.; Perry, J. K.; Goddard, W. A., III *J. Phys. Chem.* **1995**, *99*, 6340.

(62) Andersen, A.; Muntean, F.; Walter, D.; Rue, C.; Armentrout, P. B. *J. Phys. Chem. A* **2000**, *104*, 692.

(63) Zhang, X.-G.; Armentrout, P. B. *Organometallics*. Submitted for publication.

Table 3. Comparison of Experimental and Theoretical Thermochemistry for PtH_x⁺ (x = 1 and 2) and PtCH_y⁺ (y = 0–4) Species

species	this work					previous work	
	exp	theory ^a			SD	exp	theory
		HW	HW+	HW+X			
Pt ⁺ –H (¹ Σ ⁺)	2.81 ± 0.05	2.61	2.55	2.57	2.53		2.73 ^b
Pt ⁺ –H (³ Δ)		2.78	2.64	2.69	2.49		2.69 ^b
Pt ⁺ –H ₂ (² A ₁)	1.52 ± 0.12	1.68	1.60	1.66	1.48		
Pt ⁺ –CH ₃ (¹ A ₁)	2.67 ± 0.08	2.48	2.41	2.45	2.42		2.66 ± 0.22, ^c
Pt ⁺ –CH ₃ (³ E)		2.52	2.49	2.62	2.34		2.78 ± 0.22 ^c
Pt ⁺ –CH ₂ (² A ₁)	4.80 ± 0.03	4.73	4.63	4.60	4.55	4.85 ± 0.04 ^c	4.85, ^d 4.97, ^e 5.33 ± 0.22 ^f
Pt ⁺ –CH (¹ Σ ⁺)	5.56 ± 0.10	5.12	5.67	5.82	5.50		7.6 ^g
Pt ⁺ –C (² Σ ⁺)	5.43 ± 0.05	5.52	5.43	5.57	5.37		
Pt ⁺ –CH ₄ (² A ⁺) ^h	1.77 ± 0.08	1.57	1.49	1.58			1.76, ^e 1.68, ⁱ 1.59 ^j

^a Calculations using B3LYP/6-311++G(3df,3p) and the ECP indicated on Pt⁺. HW = Hay–Wadt (ref 47), HW+ = Hay–Wadt as adjusted for the cation by Ohanessian et al. (ref 19), HW+X = Hay–Wadt as adjusted for the cation by Ohanessian et al. and with extended diffuse functions as specified by Pavlov et al. (ref 9), SD = Stuttgart–Dresden (ref 48). ^b Reference 17. ^c Reference 17. ^d Calculated from data of refs 8 and 9 using the thermochemical data in Table 1. ^e Reference 10. ^f Reference 14. ^g Estimated in ref 14. ^h This species has the H–Pt⁺–CH₃ structure; see text. ⁱ Reference 9. ^j Reference 8.

of the kinetic energy distributions of the reactants. From eq 19 and $D_0(\text{D}–\text{CD}_3) = 4.58$ eV (Table 1), this threshold yields a Pt⁺–D BDE of 2.68 ± 0.06 eV. This value is a little smaller than $D_0(\text{Pt}^+–\text{D}) = 2.85 \pm 0.05$ eV obtained from the reaction of Pt⁺ with D₂³⁷ because competition with process 5 probably pushes the threshold for PtD⁺ in the CD₄ system to slightly higher energies. Similarly, $D_0(\text{Pt}^+–\text{H}) = 2.72 \pm 0.05$ eV obtained from the reaction of Pt⁺ with CH₄ is a little smaller than $D_0(\text{Pt}^+–\text{H}) = 2.80 \pm 0.08$ eV from the reaction of Pt⁺ with H₂.³⁷ Because there are no competitive processes in the reactions of Pt⁺ with H₂ and D₂, the BDEs from these two systems are believed to be our most accurate determinations. Adjustment of $D_0(\text{Pt}^+–\text{D}) = 2.85 \pm 0.05$ eV for the zero-point energy difference⁶⁴ leads to $D_0(\text{Pt}^+–\text{H}) = 2.81 \pm 0.05$ eV, in good agreement with the experimental value of $D_0(\text{Pt}^+–\text{H}) = 2.80 \pm 0.08$ eV obtained directly from the reaction of Pt⁺ with H₂.

Calculations indicate that the Pt⁺–H bond is formed by a covalent interaction between the singly occupied 5dσ orbital on Pt⁺ (89% of the bonding character with the 6s comprising 11%) and the singly occupied 1s orbital on H, such that the ground state is ¹Σ⁺.¹⁹ This bonding scheme requires no promotion from the ground electronic state of Pt⁺(²D,5d⁹) and no loss of exchange energy. Coupled with the lanthanide contraction and relativistic effects,^{6,14,19} this results in a very strong bond, as compared to first-row and second-row metal congeners.² Our experimental BDE is in good agreement with the theoretical value of 2.73 eV calculated using generalized valence bond (GVB) theory followed by correlation consistent configuration interaction (CCCI/D) calculations with a relativistic effective core potential for Pt.¹⁹ The calculations performed here provide comparable values of 2.61 (HW), 2.55 (HW+), 2.57 (HW+X), and 2.53 (SD) eV (Table 3).

The literature calculations¹⁹ also indicate that there is a low-lying ³Δ state formed from interaction of Pt⁺(⁴F,6s¹5d⁸) with H(²S,1s). Here, the bonding orbital on Pt is a 6s–5dσ hybrid (~60% d and 40% s).¹⁹ Such hybridization is particularly efficient in the third-row transition metals because relativistic effects make the 6s orbital comparable in size to the 5d orbitals. Consequently, even though binding to Pt⁺(⁴F,6s¹5d⁸) requires both promotion and the loss of exchange energy, the 6s–5dσ hybrid bonding orbital overlaps better with the 1s orbital of H, such that the ³Δ state is calculated to lie only 0.04 eV above

the ¹Σ⁺ ground state.¹⁹ Our calculations using the HW, HW+, and HW+X ECPs find that the triplet state is the ground state by 0.17, 0.09, and 0.12 eV, respectively, with bond energies close to the experimental value. The SD-ECP calculation suggests an excitation energy for the triplet state of 0.04 eV, comparable with the literature result. Clearly, the true ground state for PtH⁺ cannot be unambiguously assigned.

Pt⁺–CH₃. The BDE of Pt⁺–CH₃ derived from the CH₄ system is 2.62 ± 0.15 eV, and that of Pt⁺–CD₃ is 2.81 ± 0.05 eV from the CD₄ system. In related work concerning the reactions of Pt⁺ with larger hydrocarbons,²⁹ we have obtained values of 2.61 ± 0.10 eV from C₂H₆, 2.64 ± 0.05 eV from C₂H₄, 2.77 ± 0.05 eV from C₂D₄, and 2.63 ± 0.05 eV from CH₃OD. The average of all six values is 2.67 ± 0.08 eV for Pt⁺–CH₃ (including zero-point energy corrections of 0.03 eV for the deuterated species). Because the Pt⁺–CH₃ bond energy is similar to the experimental bond energy of Pt⁺–H at 2.81 ± 0.05 eV, there appears to be a single bond between Pt⁺ and CH₃. This identifies this species as the platinum methyl cation.

Theory also indicates that PtCH₃⁺ has a single covalent Pt–C bond.¹⁷ Here, the bonding involves the interaction between the singly occupied 5dσ orbital on Pt⁺ and the singly occupied sp³ hybridized orbital on CH₃, such that the ground state is ¹A₁.¹⁷ In direct correspondence with the PtH⁺ species, there is again a low-lying triplet state, ³E. At the B3LYP, QCISD, and QCISD(T) levels, this state lies above the ¹A₁ ground state by 0.07, 0.11, and 0.13 eV, respectively, whereas the ³E state lies below the ¹A₁ state by 0.07 eV in B3LYP calculations.¹⁷ Our B3LYP calculations find that the ³E state lies below the ¹A₁ state by 0.04 (HW-ECP), 0.08 (HW+-ECP), and 0.17 (HW+X-ECP) eV, and above the ¹A₁ state by 0.08 eV (SD-ECP). Clearly, a definitive prediction of the ground state is not possible at present.

The experimental Pt⁺–CH₃ bond energy measured here is in good agreement with theoretical values from Holthausen et al.,¹⁷ who calculated a value of 2.66 ± 0.22 eV for the ¹A₁ state at the B3LYP level, a value that includes an empirical adjustment upward of 0.22 eV, and 2.78 ± 0.22 eV for the ³E state calculated at the QCISD(T) level, which includes an empirical increase of 0.16 eV.¹⁷ Our calculations (with no empirical corrections), Table 3, yield very similar values to those obtained without the empirical adjustments. Note that the relative PtH⁺ and PtCH₃⁺ bond energies are properly described by theory compared with experiment. The former is stronger than the latter by 0.13 ± 0.09 eV, whereas theory predicts differences of 0.09 (HW-ECP), 0.06 (HW+-ECP), 0.07 (HW+X-ECP), and 0.11 eV (SD-ECP).

(64) The vibrational frequency of PtH⁺ is calculated to be 2399 cm⁻¹ (ref 19). Adjusting for the change in reduced mass, this means that PtD⁺ has a frequency of 1701 cm⁻¹, such that the zero-point energy correction is 0.043 eV.

Pt⁺–CH₂. Reaction 5 is exothermic, establishing that $D_0(\text{Pt}^+-\text{CH}_2) > 4.71$ eV and $D_0(\text{Pt}^+-\text{CD}_2) > 4.82$ eV. From the CID experiment of PtCH_2^+ with Xe, a threshold of 5.67 ± 0.16 eV is obtained for the dissociation of the Pt^+-CH_2 bond (Table 2). Conservatively, this threshold should be viewed as an upper limit. We often have found that CID experiments of strongly bound species and small molecules provide thresholds that are higher than the thermodynamic bond energies probably because of inefficiencies in the transfer of kinetic to internal energy in the collision process.⁶⁵

The best evidence that the PtCH_2^+ BDE cannot be as strong as 5.6 eV comes from reactions of PtCH_2^+ with H₂ and D₂. In both systems, formation of Pt^+ exhibits no obvious threshold, Figure 3, indicating that the dehydrogenation of methane by Pt^+ must be close to a thermoneutral process. From the rate constants for the forward and reverse reactions at the lowest kinetic energies in our experiments, we determine an equilibrium constant K of 63 ± 33 for $\text{Pt}^+ + \text{CH}_4 \rightleftharpoons \text{PtCH}_2^+ + \text{H}_2$. This compares favorably with the ratio of the forward and reverse rates determined by ICR studies, 120 ± 60 , although Heinemann et al. chose to report a value of 160 ± 80 , taken from a ratio of the reaction efficiencies.⁸ From $\Delta G = -RT \ln K$, the free energy of the reaction is calculated to be -0.11 ± 0.02 eV at 298 K, again comparable to the value of Heinemann et al. of -0.14 ± 0.04 eV.⁸ Using entropic and temperature corrections calculated by Heinemann et al., our free energy value can be converted to an enthalpy of reaction at 0 K of -0.09 ± 0.02 eV. Combining this value with the thermochemistry in Table 1 (which is slightly different than that used by Heinemann et al.), we obtain a BDE for Pt^+-CH_2 of 4.80 ± 0.03 eV, close to the value of 4.85 ± 0.04 eV reported for the ICR experiment.^{8,9}

These experimental values are in good agreement with several recent theoretical values. An early value calculated using GVB theory at the MR-CISD (multiple-reference configuration interaction including single and double excitations) level was 4.83 eV (D_e value), which was empirically corrected to a D_0 value of 5.33 ± 0.22 eV.¹⁴ A comprehensive theoretical examination of the PtCH_2^+ molecule obtained D_e values of 4.78, 4.75, and 5.20 eV at the MP2, CCSD(T), and B3LYP levels,¹⁵ respectively, when using the Hay–Wadt relativistic effective core potential (HW ECP).⁴⁷ When the shape-consistent relativistic ECP of Christiansen, Ermler, Ross, and co-workers⁶⁶ was used, values of 4.56, 4.59, and 5.01 eV, respectively, were obtained.¹⁵ All calculations at the MP2 level gave BDEs ranging from 4.37 to 4.61 eV (and gave 2.19 eV when relativistic effects were ignored). Recently, a value of 4.85 eV was obtained using the PCI-80 scheme,⁹ 4.71 eV at the B3LYP/HW-ECP/6-311+G-(2d,2p) level,⁹ and 4.97 eV at the B3LYP/SD-ECP/6-311++G-(3d,3dp) level.¹⁰ Our calculation values (using B3LYP and a 6-311++G(3df,3p) basis set on the light atoms) are 4.73 (HW-ECP), 4.63 (HW+-ECP), 4.60 (HW+X-ECP), and 4.55 (SD-ECP) eV, Table 3. (Note that the SD-ECP value, which has been corrected by 0.418 eV for the experimental spin–orbit splitting of the ²D state of Pt^+ , reproduces the 4.97 eV value from ref 10 without this correction.) Overall, it is clear that the experimental and theoretical values are in reasonable accord.

Theoretical calculations indicate that PtCH_2^+ has a ²A₁ ground state.^{14,18,67} The valence electronic configuration is $(1a_1)^2(1b_1)^2(1b_2)^2(1a_2)^2(2a_1)^2(3a_1)^1$, where the 1a₁ and 1b₁ orbitals are

bonding, the 1b₂, 1a₂, and 2a₁ orbitals are 5d nonbonding orbitals on Pt, and the 3a₁ orbital is a nonbonding 6s–5d σ hybrid orbital on Pt.¹⁴ Thus, there is a covalent double bond between Pt^+ and CH₂ but this requires the promotion of Pt^+ to the 6s¹5d⁸ electronic configuration. Spin–orbit coupling (SOC) in this molecule has recently been investigated.⁶⁷ These calculations find that SOC leads to a stabilization of about 0.14 eV for the ground state and an excitation energy to the first excited state (largely ²A₂) of 0.57 eV. Note that this stabilization largely accounts for the differences between the calculated and experimental bond energies in Table 3.

Pt⁺–CH. This ion is formed by dehydrogenation of the primary PtCH_3^+ product. Measured E_0 values (Table 2) lead to a Pt^+-CH bond energy of 5.50 ± 0.05 eV for the CH₄ system and a Pt^+-CD bond energy of 5.66 ± 0.14 eV for the CD₄ system. The two values agree with values derived from related work in our laboratory of 5.48 ± 0.05 (C₂H₄), 5.67 ± 0.10 (C₂D₄), and 5.51 ± 0.07 (C₂H₂) eV.²⁹ The average of all five values is 5.56 ± 0.10 eV after zero-point energy correction of 0.02 eV for the deuterated values and is our best experimental value for Pt^+-CH . Formation of PtCH^+ (PtCD^+) is a high energy process in all these systems, meaning that its threshold could be shifted to higher energies because of competition with lower energy reactions. However, the very good agreement among these values suggests that our analyses of the data provide accurate thermodynamic thresholds.

Irikura and Goddard used promotion energy ideas to estimate that the Pt^+-CH bond energy should be about 7.6 eV,¹⁴ well in excess of our measured value. In contrast, our calculations obtain Pt^+-CH BDEs, Table 3, that are in good accord with experiment except for the HW-ECP value of 5.12 eV. The error in this value is on the same order as the error in the ²D–⁴F state splitting for Pt^+ . These calculations (HW+-ECP) find a ¹Σ⁺ ground state with a linear geometry and $r(\text{Pt}-\text{C}) = 1.676$ Å and $r(\text{C}-\text{H}) = 1.099$ Å. Thus, a triple bond is clearly formed. A triplet state is also found with $r(\text{Pt}-\text{C}) = 1.775$ Å and $r(\text{C}-\text{H}) = 1.101$ Å and $\angle\text{PtCH} = 136.6^\circ$, indicating a lower bond order. This state is calculated to lie higher than the singlet state by 0.68 (HW-ECP), 1.19 (HW+-ECP), 1.23 (HW+X-ECP), and 1.10 (SD-ECP) eV.

Pt⁺–C. This ion is formed by dehydrogenation of the primary PtCH_2^+ product. The E_0 values measured (Table 2) lead to Pt^+-C bond energies of 5.42 ± 0.15 (CH₄ system) and 5.41 ± 0.05 (CD₄ system) eV. These values are in good agreement with values derived from related work in our laboratory of 5.42 ± 0.05 (C₂H₄), 5.45 ± 0.05 (C₂D₄), 5.47 ± 0.06 (C₂H₂), and 5.42 ± 0.07 (CO) eV.²⁹ The average of all six values is 5.43 ± 0.05 eV, taken as our best value. As for PtCH^+ , formation of PtC^+ is a high-energy process in all these systems, meaning that its threshold could be shifted to higher energies because of competition with lower energy reactions. However, the very good agreement among these values suggests that our analysis of the data provides accurate thermodynamic thresholds.

Our calculations on Pt^+-C obtain a ²Σ⁺ ground state with a Pt–C bond length of 1.678 Å (HW+-ECP). Our calculated BDEs, Table 3, are all in good agreement with experiment. Consistent with the bond energy relative to PtCH^+ , the calculated electronic configuration shows that there is essentially a triple bond formed between the σ and π 5d(Pt)–2p(C) orbitals. The unpaired electron resides in a nonbonding orbital that is largely 6s(Pt). With two unpaired electrons on C(³P), it might have been presumed that the bonding of C to Pt^+ should be similar to that of CH₂(³B₁); however, the C atom can use its empty 2p orbital to accept electron density from a doubly

(65) Sievers, M. R.; Chen, Y.-M.; Armentrout, P. B. *J. Chem. Phys.* **1996**, *105*, 6322.

(66) Ross, R. B.; Powers, J. M.; Atashroo, T.; Ermler, W. C.; LaJohn, L. A.; Christiansen, P. A. *J. Chem. Phys.* **1990**, *93*, 6654.

(67) Rakowitz, F.; Marian, C. M.; Schimmelpfennig, B. *Phys. Chem. Chem. Phys.* **2000**, *2*, 2481.

occupied 5d orbital on Pt⁺. This additional sharing of electrons can enhance the PtC⁺ bond energy empirically by 0.63 ± 0.06 eV [$= D_0(\text{Pt}^+-\text{C}) - D_0(\text{Pt}^+-\text{CH}_2)$].

H–Pt⁺–H. If the threshold for formation of PtH₂⁺ in the CH₄ system is presumed to correspond to the thermodynamic limit, then the Pt⁺–H₂ bond energy is derived as 0.66 ± 0.05 eV. Similarly, we obtain 0.74 ± 0.06 eV for Pt⁺–D₂ from the CD₄ system. However, these products have the highest thresholds observed and therefore they compete with all other products, in particular, with the much more facile formation of PtCH₂⁺ + H₂ (PtCD₂⁺ + D₂). Therefore, the derived BDEs are best viewed as lower limits. In related work,²⁹ we also have obtained values for the Pt⁺–H₂ BDE of 1.18 ± 0.05 eV from the C₂H₆ system, 1.52 ± 0.15 eV from the C₂H₄ system, and 1.52 ± 0.10 eV from the C₂D₄ system. In systems where there is competition with other reaction channels or barriers along the potential energy surface, the thresholds can be elevated, leading to BDEs that are lower than the true thermodynamic result. Therefore, we take the average of the latter two values as the most accurate thermochemistry, Table 3. This value is supported by the comparable thermochemistry measured for dissociation of PtCH₄⁺ to Pt⁺ + CH₄ (see next section).

Our calculations indicate that PtH₂⁺ is a dihydride with a ²A₁ ground state. HW+–ECP results find that the Pt–H bonds have lengths of 1.530 Å with a ∠HPtH bond angle of 83.3°. This indicates that the H–Pt⁺–H bonds are formed by covalent interaction between two singly occupied 6s–5dσ hybrid orbitals on Pt⁺ and the singly occupied 1s orbital on each H. Our calculations obtain BDEs, Table 3, in reasonable agreement with experiment, which supports the thermochemistry chosen above.

Given that the BDE for PtH₂⁺ dissociating into Pt⁺ + H₂ is 1.52 ± 0.12 eV, then the sum of the individual Pt⁺–H BDEs, $D_0(\text{HPt}^+-\text{H}) + D_0(\text{Pt}^+-\text{H}) = D_0(\text{Pt}^+-\text{H}_2) + D_0(\text{H}_2)$, is 6.00 ± 0.12 eV. From this, we determine the HPt⁺–H bond energy as about 3.19 ± 0.12 eV, which is stronger than the Pt⁺–H bond by 0.38 ± 0.12 eV. The similarity of the first and second BDEs is consistent with a dihydride species, and is comparable to our results for the PtCH₄⁺ species, identified experimentally to have a H–Pt⁺–CH₃ structure. The enhanced strength of the second bond is reasonable once we consider promotion and exchange energies needed to form these covalent bonds. As noted above, calculations indicate that the Pt⁺–H BDEs are similar for the ¹Σ⁺ and ³Δ states. The latter is formed by interaction of H(²S,1s) with Pt⁺(⁴F,6s¹5d⁸), which requires a promotion energy of 0.76 eV³⁶ and an exchange energy loss of about 0.55 eV to form the first Pt⁺–H bond. The second bond requires no additional promotion and an exchange energy loss of about 0.84 eV, such that the second bond should be about 0.47 eV stronger than the first, consistent with observation.

H–Pt⁺–CH₃. The production of PtH⁺ from the CID experiment of PtCH₄⁺ with Xe strongly suggests that this species has a H–Pt⁺–CH₃ structure. In previous CID experiments of M⁺–(CH₄) with Xe, only M⁺ products are observed,^{58,60,61} indicating that the M⁺(CH₄) species in these cases are probably simple adducts. From the CID experiment of PtCH₄⁺ with Xe, a threshold of 1.72 ± 0.05 eV (Table 2) is obtained for the Pt⁺ + CH₄ channel. Alternatively, from the threshold for formation of PtH⁺ + CH₃ (Table 2) combined with the thermochemistry for PtH⁺ given above (Table 3) and values in Table 1, we determine that dissociation of PtCH₄⁺ to Pt⁺ + CH₄ requires 1.83 ± 0.08 eV. Overall, our best determination of the stability of PtCH₄⁺ comes from an average of the two experimental values, 1.77 ± 0.08 eV, where the uncertainty is two standard deviations of the mean. Given this value, the sum of both

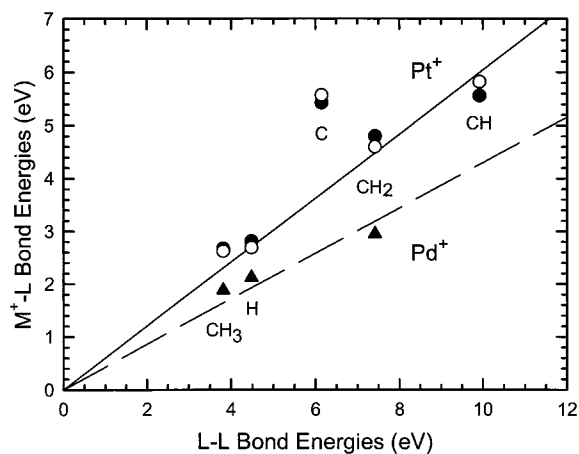


Figure 5. Correlation of Pt⁺–L and Pd⁺–L bond energies with those for the organic analogues, L–L. Pt⁺–L values are from Table 3 and include both experiment (closed circles) and theory (HW+–X, open circles). Pd⁺–L values (triangles) are from ref 22. Lines are linear regression fits to the experimental data, excluding Pt⁺–C, constrained to pass through the origin to emphasize the bond-order correlations.

H–Pt⁺–CH₃ bonds is 6.23 ± 0.08 eV. Thus, the HPt⁺–CH₃ bond is about 3.42 ± 0.09 eV, in good agreement with the direct measurement of the CID of PtCH₄⁺ to PtH⁺ (Table 2), 3.50 ± 0.06 eV. In addition, the CH₃Pt⁺–H bond is calculated to be 3.55 ± 0.10 eV. Both of these bonds are stronger than the first bond energies, Pt⁺–CH₃ and Pt⁺–H, respectively, by 0.74 eV. As noted in the previous section, this can be attributed to the difference in promotion and exchange energies for formation of the first and second bonds.

The experimental stability of PtCH₄⁺ agrees well with values calculated for a H–Pt⁺–CH₃ intermediate of 1.68 eV obtained using the PCI-80 scheme,⁹ 1.59 eV at the B3LYP/HW-ECP/6-311+G(2d,2p) level^{8,9} and 1.76 eV at the B3LYP/SD-ECP/6-311++G(3d,3dp) level.¹⁰ Our calculation values (using B3LYP and a 6-311++G(3df,3p) basis set on the light atoms) are 1.57 (HW-ECP), 1.49 (HW+–ECP), and 1.58 (HW+X-ECP) eV, also in reasonable agreement. Our experimental BDE does not correspond well with values of 1.10 (PCI-80),⁹ 0.83 (B3LYP/HW-ECP),⁹ and 1.31 (B3LYP/SD-ECP) eV,¹⁰ or our values of 0.92 (HW-ECP), 0.85 (HW+–ECP), and 0.90 (HW+–ECP) eV calculated for the Pt⁺(CH₄) adduct relative to Pt⁺ + CH₄. This further verifies the structural identity of the ground-state PtCH₄⁺ species formed in the flow tube.

Ab initio calculations indicate that H–Pt⁺–CH₃ has a ²A' ground state, with a 90.7° bond angle between the two ligands.⁸ (Other literature theoretical calculations do not explicitly report this bond angle, but the structures shown clearly indicate similar geometries.^{9,10}) Our HW+–ECP calculations obtain the same ground state with a 91.6° bond angle. This geometry indicates that the covalent bonds are formed using the two 6s–5dσ hybrid orbitals on Pt⁺, which requires promotion to Pt⁺(⁴F,6s¹5d⁸).

Bond-Energy Bond-Order Correlation for Pt⁺–CH_x Bonds.

One interesting way of investigating the bond order of simple metal–ligand species is to compare with organic analogues, i.e., $D_0(\text{Pt}^+-\text{L})$ versus $D_0(\text{L}-\text{L})$.⁶⁸ Such a plot is shown in Figure 5. It can be seen that the correlation is remarkably good, which indicates that Pt⁺–H and Pt⁺–CH₃ are single bonds, Pt⁺=CH₂ is a double bond, and Pt⁺≡CH is a triple bond. (The linear regression line in Figure 5 is constrained to include the origin to emphasize the bond-order correlation of the PtL⁺ vs L₂ species. A reviewer correctly notes that this constraint is not

Table 4. Experimental and Theoretical Thermochemistry (in eV) for Various $[\text{Pt},\text{C},\text{H}_4]^+$ Species

species	experiment	theory ^a					
		present results			literature		
		B3LYP/TZ-HW	B3LYP/TZ-HW+	B3LYP/TZ-HW+X	PCI-80 ^b	B3LYP/DZ-HWX ^b	B3LYP/TZ-SD ^c
$\text{Pt}^+ + \text{CH}_4$	1.77 (0.08)	1.573	1.493	1.580	1.683	1.591	1.759
$\text{Pt}^+ - \text{CH}_4$		0.656	0.640	0.677	0.582	0.758	0.453
TS1		0.742	0.759	0.767	0.508	0.672	0.473
$\text{H} - \text{Pt}^+ - \text{CH}_3$	0.0	0.0	0.0	0.0	0.0	0.0	0.0
TS2		1.050	1.077	1.032	1.067	1.136	1.015
$(\text{H}_2)\text{PtCH}_2^+$		0.823	0.844	0.799	0.946	0.923	0.801
TS3		1.154	1.173	1.102	1.241	1.313	1.080
$(\text{H}_2)\text{PtCH}_2^+$		0.993	0.983	0.927	0.963	0.915	0.920
$\text{PtCH}_2^+ + \text{H}_2$	1.68 (0.09)	1.509	1.529	1.640	1.501	1.556	1.498
<i>d</i>	-0.09 (0.03)	-0.064	+0.036	+0.060	-0.182	-0.035	-0.261

^a DZ/TZ = double/triple- ζ basis set used in geometry optimizations. HW = Hay–Wadt ECP (ref 47), HWX = Hay–Wadt as adjusted for the cation by Ohanessian et al. (ref 19), HWX = Hay–Wadt with extended diffuse functions as specified by Pavlov et al. (ref 9), SD = Stuttgart–Dresden ECP (ref 48). ^b Reference 9. ^c Reference 10. To accurately compare with experiment, these values may need to be corrected by adding 0.418 eV to account for the spin–orbit states of $\text{Pt}^+(^2\text{D})$. ^d Energies relative to $\text{Pt}^+ + \text{CH}_4$. Spin–orbit coupling effects could lower the theoretical values by about 0.14 eV (ref 67).

necessary and that correlations between $D_0(\text{Pt}^+ - \text{CH}_4) \approx 0.9$ eV and $D_0(\text{CH}_4 - \text{CH}_4) \approx 0.0$ eV could also be included to good effect.) The point that lies furthest from the line is for $\text{Pt}^+ - \text{C}$, correlated with the BDE of C_2 . In this case, the $\text{Pt}^+ - \text{C}$ BDE is stronger than predicted by this simple correlation because the covalent double bond in this molecule can be augmented by back-donation of an occupied 5d orbital on Pt^+ into the empty 2p orbital on C. Such an interaction cannot occur in the C_2 molecule.

Also illustrated in Figure 5 is the remarkably good agreement between experiment and theory. Indeed, we find that all four sets of theoretical values in Table 3 deviate from experiment by only 0.16 eV (mean absolute deviation).

Potential Energy Surface of $[\text{PtCH}_4]^+$. In constructing a potential energy surface (PES) for the interaction of $\text{Pt}^+(^2\text{D}_{5/2}) + \text{CH}_4(^1\text{A}_1)$, we first consider the spin states of all the various product channels. Ab initio calculations indicate that the ground states of all intermediates and transition states leading to the $\text{PtCH}_2^+(^2\text{A}_1) + \text{H}_2(^1\Sigma_g^+)$ products have doublet-spin ground states.⁸ Thus, the dehydrogenation process is spin-allowed, as is the complementary formation of $\text{PtH}_2^+(^2\text{A}_1) + \text{CH}_2(^3\text{B}_1)$. The subsequent dehydrogenation, $\text{PtCH}_2^+(^2\text{A}_1) \rightarrow \text{PtC}^+(^2\Sigma^+) + \text{H}_2(^1\Sigma_g^+)$, is also spin-allowed. In addition, formations of $\text{PtH}^+ + \text{CH}_3(^2\text{A}_2'')$ and $\text{PtCH}_3^+ + \text{H}(^2\text{S}_{1/2})$ are spin-allowed whether the ions are formed in singlet or triplet states. The subsequent dehydrogenation process of $\text{PtCH}_3^+ \rightarrow \text{PtCH}^+ + \text{H}_2$ is spin-allowed as long as both ions have the same spin. Therefore, all reaction processes observed here for the activation of methane by Pt^+ are spin-allowed.

The PES for the dehydrogenation of methane by Pt^+ has been investigated thoroughly in the literature using PCI-80⁹ and B3LYP^{8–10} approaches. The literature B3LYP calculations differ in that one involves geometry optimizations using a double- ζ basis set on C and H and the Hay–Wadt ECP followed by single point calculations using a triple- ζ 6-311+G(2d,2p) basis on C and H and an extended basis on Pt (B3LYP/DZ-HW-ECP),^{8,9} whereas the other utilizes a triple- ζ 6-311++G(3d,3dp) basis set on C and H and the Stuttgart–Dresden ECP on Pt for both geometry optimizations and energies (B3LYP/TZ-SD-ECP).¹⁰ Our calculations were pursued primarily to provide consistent theoretical treatments of the higher energy channels observed in these experiments, with thermochemistry summarized in Table 3, but the PtCH_4^+ species previously investigated were also examined. Our calculations used B3LYP and a 6-311++G(3df,3p) basis set on C and H for both geometry optimizations and energetics along with several variations of the Hay–Wadt

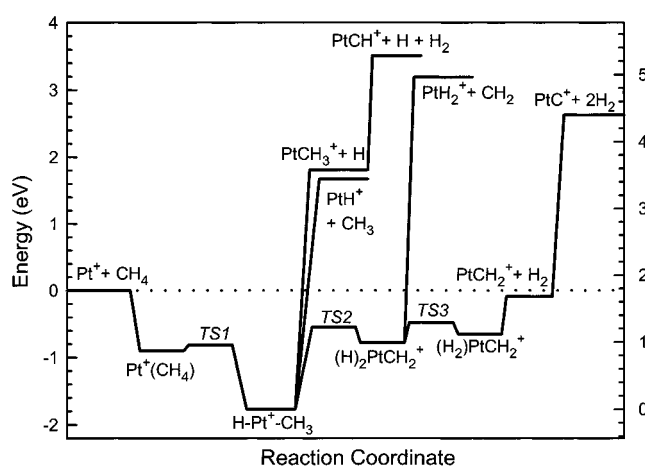


Figure 6. $[\text{PtCH}_4]^+$ potential energy surface derived from experimental and theoretical results. The relative energies of $\text{Pt}(\text{CH}_4)^+$, TS1, TS2, $(\text{H}_2)\text{PtCH}_2^+$, TS3, and $(\text{H}_2)\text{PtCH}_2^+$ are based on ab initio calculations (HW+X-ECP, see Table 4). All other values are experimental and taken from Table 3. Energies on the left are relative to the $\text{Pt}^+ + \text{CH}_4$ asymptote, whereas those on the right are referenced to the HPtCH_3^+ intermediate.

ECP, as described above. Calculations concerning the PtCH_4^+ species using the SD-ECP did not converge readily and hence were not pursued further. Results for the literature calculations along with the present values are compiled in Table 4. In all cases, the values have been corrected for zero-point energies.

Using experimental values where possible along with the HW+X-ECP results from our work, we construct a potential energy surface for the reaction of Pt^+ with methane as shown in Figure 6. The initial interaction of Pt^+ with CH_4 is attractive because of the long-range ion–induced dipole interaction.^{2,40} Thus, there is a potential well corresponding to the $\text{Pt}^+(\text{CH}_4)$ adduct, which has C_s geometry and $^2\text{A}'$ ground state according to theoretical calculations.⁸ The depth of this potential well is about 0.9 eV relative to the reactants, Table 4. As the reactants approach more closely, the system passes through a transition state (TS1) as Pt^+ inserts into one C–H bond of CH_4 to form the $\text{H} - \text{Pt}^+ - \text{CH}_3$ intermediate. Calculations find a barrier relative to the adduct of only 0.03 ± 0.09 eV, and several of the calculations find no barrier.

As noted above, our experiment determines the ground state of the $\text{H} - \text{Pt}^+ - \text{CH}_3$ intermediate to be 1.77 ± 0.08 eV below the ground state of reactants, in agreement with theoretical calculations (Tables 3 and 4). The HPtCH_3^+ intermediate

evolves into the $(H)_2PtCH_2^+$ intermediate by passing through transition state TS2. TS2, a three-centered transition state involving migration of an H-atom from C to Pt, lies about 1.1 eV higher than the $HPtCH_3^+$ intermediate and about 0.5 eV below reactants. The $(H)_2PtCH_2^+$ intermediate is about 0.7 eV below the reactants, much higher than the value of 1.6 ± 0.1 eV estimated from simple bond additivity as $D_0(Pt^+-CH_2) + D_0(H-Pt^+-H)$. This is because the maximum number of covalent bonds that Pt^+ can form is three, such that the $(H)_2PtCH_2^+$ intermediate has two σ Pt^+-H bonds and one σ Pt^+-CH_2 bond, but the Pt^+-CH_2 π -interaction involves three electrons (one in an antibonding orbital), as confirmed by our calculations.

The next step in the dehydrogenation process is reductive elimination of H_2 from $(H)_2PtCH_2^+$ to form $(H)PtCH_2^+$ with a transition state (TS3) between them. The latter intermediate is about 0.1 eV higher than the former and TS3 lies about 0.3 eV higher than the $(H)_2PtCH_2^+$ intermediate (about 0.4 eV below reactants). The last step in the dehydrogenation process is the loss of H_2 from the $(H)PtCH_2^+$ intermediate, which proceeds without a barrier to the $PtCH_2^+ + H_2$ asymptote. The production of $PtCH_2^+ + H_2$ is exothermic by 0.09 ± 0.02 eV relative to the reactants according to our experiments, in reasonable agreement with theory, Table 4. Note that including a spin-orbit coupling stabilization to $PtCH_2^+$ of 0.14 eV⁶⁷ to the theoretical values would bring several of them into better agreement with experiment.

Discussion

σ -bond activation by atomic metal ions can be understood using a simple donor-acceptor model. Simply, such reactions require electronic configurations in which there is an empty acceptor orbital on the metal ion into which the electrons of a bond to be broken are donated. Concomitantly, metal electrons in orbitals having π -symmetry back-donate into the antibonding orbital of the bond to be broken. If the acceptor orbital is occupied, a repulsive interaction can result leading to inefficient reaction either by more direct abstraction pathways or by introduction of a barrier to the reaction.

In our previous studies, the activation of methane by atomic metal ions was explained by this simple donor-acceptor model, which leads to an oxidative addition mechanism.² In such a mechanism,⁵¹⁻⁵⁸ oxidative addition of a C-H bond to M^+ forms a $H-M^+-CH_3$ intermediate. Products can be formed by the reductive elimination of H_2 at low energies, by metal-hydrogen or metal-carbon bond cleavage at high energies, and by further dehydrogenation of primary products at still higher energies. For first-row transition metal ions,² the reductive elimination process proceeds through a four-centered transition state from $H-M^+-CH_3$ intermediate to $(H)MCH_2^+$ intermediate in which a hydrogen molecule is electrostatically bound to the MCH_2^+ species. This latter intermediate then decomposes by expulsion of H_2 . However, as outlined above, *ab initio* calculations of the potential energy surface for dehydrogenation of methane by Pt^+ indicate a different reaction mechanism.⁸⁻¹⁰

Mechanism for Reaction of Pt^+ with Methane. All processes observed in the reaction of Pt^+ with methane can be understood using the mechanism shown on the potential energy surface (PES) in Figure 6. Oxidative addition of CH_4 to Pt^+ produces a hydrido-methyl platinum cation intermediate, $H-Pt^+-CH_3$, the global minimum on the potential energy surface. This process is efficient and essentially barrierless, Figure 6, because the empty 6s orbital on $Pt^+(^1D)$ acts as an efficient acceptor orbital and one of the doubly occupied 5d π orbitals provides

an efficient donor orbital. This leads naturally to an intermediate in which the Pt^+ forms two bonds using 6s-5d hybrids. At the lowest energies, the activation of a second C-H bond (α -H transfer) leads to formation of dihydrido-methylidene platinum cation intermediate, $(H)_2PtCH_2^+$, which then reductively eliminates dihydrogen to form the $(H_2)Pt^+(CH_2)$ intermediate, an electrostatic complex. This species decomposes to form the platinum carbene cation, Pt^+-CH_2 , by loss of H_2 in an overall exothermic process. This mechanism and PES have been discussed thoroughly in the literature.⁸⁻¹⁰

As the energy available increases above about 2 eV, Pt^+-H and Pt^+-CH_3 products are formed by simple bond cleavages of the $H-Pt^+-CH_3$ intermediate. These processes, in particular formation of $PtH^+ + CH_3$, deplete the population of this intermediate such that the cross section for the dehydrogenation process declines commensurately. Because formation of $PtCH_2^+ + H_2$ is thermodynamically preferred by more than 1.76 eV (Tables 1 and 3), this competition indicates that formation of $PtH^+ + CH_3$ must be preferred kinetically. This is consistent with a simple bond cleavage of HPt^+-CH_3 at elevated kinetic energies, whereas the elimination of H_2 occurs via the more restricted transition states, TS2 and TS3.

In the reaction of Pt^+ with CH_4 (CD_4), the PtH^+ (PtD^+) cross section is dominant at energies above 2.5 eV (Figure 1). This is typical behavior for the reaction of bare metal ions with hydrogen-containing polyatomic molecules.^{2,5,22,51-58} The observation that the $PtH^+ + CH_3$ ($PtD^+ + CD_3$) channel dominates the nearly isoenergetic $PtCH_3^+ + H$ ($PtCD_3^+ + D$) channel is a result of angular momentum constraints.^{2,5,51,53,56} Briefly, because the $PtCH_3^+ + H$ ($PtCD_3^+ + D$) channel has a reduced mass of 1.0 (2.0) amu, much smaller than that of the reactants, 14.8 (18.2) amu, it can only be formed by the reactants that come together with smaller orbital angular momenta, i.e., at small impact parameters. In contrast, the $PtH^+ + CH_3$ ($PtD^+ + CD_3$) channel has a reduced mass of 14.0 (16.5) amu, close to that of the reactants, such that most impact parameters leading to strong interactions between the Pt^+ and methane can form these products and still conserve angular momentum. We further note that the branching ratio of $\sigma(PtD^+)/\sigma(PtCD_3^+)$ is about 45 above 3 eV, larger than the range of 4-20 suggested as appropriate for a statistical mechanism.^{5,51} The magnitude of this effect suggests that the $D-Pt^+-CD_3$ intermediate is probably short-lived at such high energies and there are contributions from a direct abstraction mechanism for the production of PtD^+ .

At high energies, PtC^+ and $PtCH^+$ are formed by dehydrogenation of the primary products, $PtCH_2^+$ and $PtCH_3^+$. The thermochemistry determined above (Tables 1 and 3) shows that these dehydrogenations require 2.72 ± 0.05 and 1.70 ± 0.10 eV, respectively. In addition, H atom loss from $PtCH_3^+$, which requires 2.60 ± 0.10 eV (Tables 1 and 3), leads to the second feature in the $PtCH_2^+$ cross section. This process is observed because the simple bond cleavage is kinetically more favorable at high energies than the more complex dehydrogenation processes. Comparable observations have been made for second-row metal systems.^{22,56,58,69,70}

The highest energy process observed experimentally is formation of $PtH_2^+ + CH_2$. It seems unlikely that this species is formed from the $(H_2)Pt^+(CH_2)$ intermediate, because H_2 is bound to Pt^+ much less strongly than methylene (BDEs of 1.52 vs 4.80 eV) and cleavage of the electrostatic $Pt^+(H_2)$ bond is a

(69) Chen, Y.-M.; Armentrout, P. B. *J. Am. Chem. Soc.* **1995**, *117*, 9291.
(70) Armentrout, P. B.; Chen, Y.-M. *J. Am. Soc. Mass Spectrom.* **1999**, *10*, 821.

dynamically much more favorable process than breaking the covalent Pt^+-CH_2 bond. However, CH_2 could be lost from the $(\text{H})_2\text{Pt}^+(\text{CH}_2)$ intermediate to produce the $\text{H}-\text{Pt}^+-\text{H}$ dihydride. CH_2 loss is more favorable thermodynamically from the $(\text{H})_2\text{PtCH}_2^+$ complex because the Pt^+-CH_2 π -interaction is already disrupted. CH_2 loss is more favorable dynamically because of the angular momentum considerations discussed above for the dominance of PtH^+ and because it is a simple bond cleavage whereas H_2 loss involves the recombination of two H atoms over a tight transition state. Thus, the observation of PtH_2^+ product in the platinum system provides evidence for a reaction pathway involving the $(\text{H})_2\text{Pt}^+(\text{CH}_2)$ intermediate.

Mechanism for the Reverse Reaction, $\text{PtCH}_2^+ + \text{H}_2$. The potential energy surface of Figure 6 also allows the reverse reaction of $\text{PtCH}_2^+ + \text{H}_2$ (D_2) to be understood in detail. Scrambling of the isotopes to form PtCHD^+ and PtCD_2^+ cannot occur from the intermediates analogous to $(\text{H})_2\text{PtCH}_2^+$ and $(\text{H})_2\text{-PtCH}_2^+$, but can only proceed from the $\text{H}-\text{Pt}^+-\text{CH}_3$ intermediate. Addition of D_2 to PtCH_2^+ would initially form a $\text{D}-\text{Pt}^+-\text{CH}_2\text{D}$ intermediate, which can reductively eliminate either D_2 to return to reactants or HD to form the dominant PtCHD^+ product, Figure 3, via a $(\text{H})(\text{D})\text{PtCHD}^+$ intermediate. Competing with this is the more energetic loss of CH_2D_2 to yield Pt^+ . At higher energies, the $\text{D}-\text{Pt}^+-\text{CH}_2\text{D}$ intermediate can decompose to form $\text{PtCH}_2\text{D}^+ + \text{D}$ and $\text{PtD}^+ + \text{CH}_2\text{D}$. Alternatively, the $(\text{H})(\text{D})\text{PtCHD}^+$ intermediate can form $\text{H}-\text{Pt}^+-\text{CHD}_2$ from which H_2 can be eliminated to yield PtCD_2^+ at low energies, or $\text{PtCHD}_2^+ + \text{H}$ and $\text{PtH}^+ + \text{CHD}_2$ can be formed at higher energies. These latter three ionic products are less abundant than the analogous species, PtCHD^+ , PtCH_2D^+ , and PtD^+ , formed from the $\text{D}-\text{Pt}^+-\text{CH}_2\text{D}$ intermediate because this intermediate must be formed prior to the rearrangement that yields the $\text{H}-\text{Pt}^+-\text{CHD}_2$ intermediate.

The activation of dihydrogen by PtCH_2^+ can also be thought of using the acceptor-donor concept and this provides more insight into the dehydrogenation reaction 5 as well. As noted above,¹⁸ the $^2\text{A}_1$ ground state of PtCH_2^+ has an electron configuration of $(1a_1)^2(1b_1)^2(1b_2)^2(1a_2)^2(2a_1)^2(3a_1)^1$. The only reasonable acceptor orbital is the partially occupied $3a_1$ orbital, largely a $6s$ orbital on Pt with some $6s-5d$ hybridization. The occupation of the $3a_1$ acceptor orbital means that the $\text{Pt}-\text{C}$ π bond is disrupted, such that the $(\text{H})_2\text{PtCH}_2^+$ intermediate is a relatively high-energy species compared to the $\text{H}-\text{Pt}^+-\text{CH}_3$ intermediate. (Other possible acceptor orbitals are all antibonding in character, leading to more severe disruption of the PtCH_2^+ species.) The donor orbital on Pt that interacts with the antibonding orbital of H_2 is the doubly occupied $2a_1$ nonbonding orbital, essentially $5d(x^2-y^2)$. These donor-acceptor interactions lead to the oxidative addition of H_2 to the Pt^+ center of PtCH_2^+ via a three-centered transition state (TS3). This contrasts with the key transition state for the comparable reaction involving first-row and second-row transition metal systems, where H_2 adds across the M^+-CH_2 bond via a four-centered transition state.²

Reactivity Differences between Pt^+ and Pd^+ Systems. Pt^+ exhibits much greater reactivity toward methane than any ions of the first-row and second-row metals.^{2,5,22,51-58} To characterize these differences, we explicitly compare the present results with comparable studies of the kinetic energy dependence of the reaction of CH_4 with Pd^+ , another group 10 metal ion.²² Unfortunately, similar work on reactions of Ni^+ with CH_4 has not yet been pursued. The differences in reaction behavior between platinum and palladium systems can be summarized succinctly. First, the bonding of Pt^+ with H and CH_3 is stronger

than that of palladium analogues by 0.7 ± 0.1 eV,²² as shown in Figure 5. In addition, the bond energy of Pt^+-CH_2 is 1.85 eV higher than that of the palladium analogue. The thermochemistry of PdCH^+ and PdC^+ has not been characterized because these species are not formed readily, probably a consequence of weak bonds. However, bond strengths of Pt^+-CH and Pt^+-C are much stronger than those of other first-row and second-row transition metals.² Second, in contrast to the behavior observed here, the dehydrogenation reaction is endothermic and relatively inefficient for the palladium system because there is a barrier in excess of the endothermicity. Third, subsequent dehydrogenation of primary products to form MC^+ and MCH^+ is pronounced in the platinum system, but such products are not observed in the palladium system. Fourth, the platinum dihydride cation is observed here but no PdH_2^+ is observed in the palladium system.

All of these differences can be understood on the basis of sd hybridization. For Pd^+ , such hybridization is inefficient because the $5s^04d^9 \rightarrow 5s^14d^8$ promotion energy is very high, 3.19 eV.³⁶ However, in the platinum system, the $6s^05d^9 \rightarrow 6s^15d^8$ promotion energy is only 0.76 eV,³⁶ largely because of relativistic effects, which also help make the sizes of the $6s$ and $5d$ orbitals comparable,^{6,14} such that sd hybridization is efficient and energetically accessible. sd hybridization is required to form multiple bonds to Pt^+ and Pd^+ , helping to explain the gross differences in thermochemistry. Such thermodynamic differences also stabilize the various transition states and intermediates along the dehydrogenation pathway for Pt^+ , enabling this reaction to occur efficiently at room temperature. In the palladium system, the inability to form multiple bonds means that the $(\text{H})_2\text{PdCH}_2^+$ intermediate is not stable, thus a four-centered transition state is postulated to exist at an energy in excess of the endothermicity to the dehydrogenation process.²² Such four-centered processes have been found to be the rate-limiting step in theoretical studies of late first-row transition metal systems (Fe and Co)^{20,71-75} and are consistent with experimental findings.^{52,55,57,76-78} Similarly, further dehydrogenation of primary products and the production of a stable dihydride species in the platinum system are consequences of the enhanced thermodynamic stability afforded by the accessibility of the s^1d^8 configuration and efficient sd hybridization.

Conclusions

Ground-state Pt^+ ions are found to be highly reactive with methane over a wide range of kinetic energies. At low energies, dehydrogenation is efficient, exothermic, and a dominant process. At high energies, the dominant process is formation of $\text{Pt}^+-\text{H} + \text{CH}_3$, which occurs mainly by simple bond cleavage of the $\text{H}-\text{Pt}^+-\text{CH}_3$ intermediate, with some contributions from a direct mechanism. This channel is favored over the isoenergetic $\text{Pt}^+-\text{CH}_3 + \text{H}$ channel because of angular momentum constraints. PtH_2^+ , which finds no analogy in the product spectrum for first-row and second-row transition metal systems,

(71) Perry, J. K. Ph.D. Thesis, Caltech, 1994.

(72) Holthausen, M. C.; Fiedler, A.; Schwarz, H.; Koch, W. *J. Phys. Chem.* **1996**, *100*, 6263.

(73) Holthausen, M. C.; Koch, W. *Helv. Chim. Acta* **1996**, *79*, 1939.

(74) Holthausen, M. C.; Koch, W. *J. Am. Chem. Soc.* **1996**, *118*, 9932.

(75) Yi, S. S.; Blomberg, M. R.; Siegbahn, P. E. M.; Weisshaar, J. C. *J. Phys. Chem.* **1998**, *102*, 395.

(76) Haynes, C. L.; Fisher, E. R.; Armentrout, P. B. *J. Am. Chem. Soc.* **1996**, *118*, 3269.

(77) Haynes, C. L.; Fisher, E. R.; Armentrout, P. B. *J. Phys. Chem.* **1996**, *100*, 18300.

(78) van Koppen, P. A. M.; Brodbelt-Lustig, J.; Bowers, M. T.; Dearden, D. V.; Beauchamp, J. L.; Fisher, E. R.; Armentrout, P. B. *J. Am. Chem. Soc.* **1991**, *113*, 2359.

is observed at high energies. This observation is suggested to imply a dihydride structure and provides evidence for the reaction pathway involving the $(H)_2PtCH_2^+$ intermediate.

Analysis of the kinetic energy dependence of the reaction cross sections provides the BDEs of Pt^+-H , Pt^+-CH_3 , Pt^+-CH_2 , Pt^+-CH , Pt^+-C , and $H-Pt^+-CH_3$. These platinum–ligand bonds are stronger than corresponding ones of first-row and second-row transition metals, which is attributed to the accessibility of the s^1d^8 electronic configuration and effective sd hybridization, a consequence of relativistic effects. Our experimental BDEs are found to be in good agreement with a variety of *ab initio* calculations, from the literature and performed here. Such calculations are also used to provide a detailed potential energy surface for the $PtCH_4^+$ system.

This potential energy surface shows that the reaction of Pt^+ with methane proceeds via the oxidative addition of one C–H bond to yield a hydrido-methyl platinum intermediate, $H-Pt^+-CH_3$, the global minimum. Pt^+-H and Pt^+-CH_3 can be formed

by simple bond cleavages from this intermediate. The activation of a secondary C–H bond proceeds through a three-centered transition state involving migration of an H-atom from C to Pt (α -H transfer) to form a $(H)_2PtCH_2^+$ intermediate. Reductive elimination of H_2 forms the electrostatic complex, $(H_2)PtCH_2^+$, from which H_2 is eliminated to form the metal carbene complex, Pt^+-CH_2 . We believe that PtH_2^+ is produced by expulsion of CH_2 from $(H)_2PtCH_2^+$. Pt^+-C and Pt^+-CH are formed by the dehydrogenation of Pt^+-CH_2 and Pt^+-CH_3 , respectively.

Acknowledgment. This work was supported by the National Science Foundation under Grant CHE9877162. X.-G. Zhang thanks Chad Rue and Felician Muntean for technical help with the experiments. We thank Detlef Schröder, Karl Irikura, Gereon Niedner-Schatteburg, and the reviewers for helpful discussions and useful comments.

JA010382O